TECHNICAL MEMORANDUMS

NATIONAL ADVISORY COMMITTEE FOR AERONAUTICS

No. 698

DYNAMIC BREAKING TESTS OF AIRPLANE PARTS

By Heinrich Hertel

Zeitschrift für Flugtechnik und Motorluftschiffahrt
Vol. 22, Nos. 15 and 16, August 14, and 28, 1931
Verlag Von R. Oldenbourg, München und Berlin

Washington
January, 1933

NATIONAL ADVISORY COMMITTEE FOR AERONAUTICS

TECHNICAL MEMORANDUM NO. 698

DYNAMIC BREAKING TESTS OF AIRPLANE PARTS*

By Heinrich Hertel

I. OBJECT OF DYNAMIC INVESTIGATIONS

The static stresses of airplane parts, the magnitude of which can be determined with the aid of static load assumptions, are mostly superposed by dynamic stresses, the magnitude of which has been but little explored. The object of the present investigation is to show how the strength of airplane parts can best be tested with respect to dynamic stresses with and without superposed static loading, and to what extent the dynamic strength of the parts depends on their structural design.

The dimensions of airplane parts are now based almost exclusively on static calculations. The stresses calculated from the adopted static loads must at no point exceed the permissible stress for the given material. The stress at the 0.2 limit of the material is regarded as the maximum permissible stress for 1.35 times the "safe load." The breaking stress of the material may be reached under the "requisite breaking load," and the safety factor against buckling of the parts under compression may sink to 1.

A few rules are given in the building specifications for the permissible stressing of the structural parts which are subjected to regular fluctuations in stress. In particular, attention is called to the fact that the special conditions due to shaping, notching, threading, etc., and in working the material must be taken into account. This effect of local stress concentration and the working of the material on the dynamic strength of a finished airplane part was investigated by vibration tests. It was found that, in metal construction, the dynamic strength of finished parts was unexpectedly small, due to the coincidence of various unfavorable conditions at places where the cross sections of riveted members change abruptly. The dynamic

*"Dynamische Bruchversuche mit Flugzeugbauteilen." Z.F.M., August 14, pp. 465-473, and August 28, pp. 489-502, 1931.

strength of airplane parts should therefore be increased by suitable structural design. In static-strength calculations no account is taken of local stress concentrations, which occur at places of abrupt change of cross section, notches, edges of holes, rivets, etc. Such neglect is customary and permissible in static-strength calculations even for high buildings and bridges, since the inherent properties of the material prevent any premature break due to local stresses. The material stressed beyond the proportionality limit at points of stress concentration becomes softer and begins to flow at the yield point, thereby avoiding any further increase in stress which might cause rupture. In a structural member stressed to the point of rupture, the points of local stress concentration precede the stresses in the undisturbed cross section only until they reach the yield point. There then occurs, with increasing load, a better and often perfect equalization of the stresses, so that the static breaking strength of the member is not impaired by the local stresses. Since the endurance limit of the materials is below the yield point and in general also below the proportionality limit, the possible stress balance no longer avails in frequently recurring loads (dynamic stresses) after a local passing of the yield point. The material becomes fatigued at the points of local stress concentration, even under alternating loads which, in the undisturbed cross section, develop stresses far below the endurance strength of the material. A dynamic break then runs from the point of disturbance (e.g., a stressed rivet hole) and leads to the rupture of the whole cross section.

Although in airplane construction, the wing and control-surface flutter must be absolutely prevented by making these structures sufficiently rigid, and other dangerous vibrations, generated by the engine, propeller or separation phenomena, should be prevented as much as possible, nearly all the structural parts of an airplane are nevertheless subject to some form of unavoidable dynamic stresses. Here we will only mention:

1. Alternating stresses produced throughout the whole airplane by gusts and by taxying on rough ground, the alternations being of low frequency, so that failures can occur only after long operation,

2. Unavoidable high-frequency vibrations of the engine bed, due to the "unbalances" of the engine, as also the alternating stresses of the

engine bed due to obliqueness of the air current with respect to the propeller,

3. Vibration of struts exposed to the air current.

No exact knowledge of the dynamic stresses of airplanes exists. Recently, however, instruments (optographs and scratch instruments) have been developed for recording dynamic stresses.

In the construction of wooden airplanes, local disturbances of the tension, which are unfavorable for dynamic loads, have long been avoided. Reinforcing strips and fitting blocks are tapered gradually. Even splices are made so as to produce no notch effect. The attachment fittings join the fitting blocks, which effect a substantial reduction of the total spar stresses. The local stress concentrations can be easily avoided in wood construction, since wood is easily shaped. The cross-sectional transitions and connections can be favorably shaped, due to the large cross-sectional areas required in wood construction. Above all, the glue used for combining wooden parts affords a uniform transmission of the stresses to all parts of the connecting surfaces.

In metal airplane construction, on the contrary, local stress concentrations in the structural parts are very hard to avoid. Especially in sheet-metal construction, i.e., in the use of metal plates and tube walls 0.3 to 2 mm (0.012 to 0.079 in.) thick, the making of gradual cross-sectional transitions is very difficult. Thus far hardly any attempt has been made to overcome these difficulties, all the more since structural engineers for bridges and high buildings have become accustomed to abrupt cross-sectional transitions. The problem is partially solved by the use of welding in steel construction, which avoids the stress increments around the rivets. It is also partially solved by elektron, with which relatively large cross-sectional areas are possible and which is very easily shaped.

Many tests have been made of the endurance strength of materials in the preferred state of the test bar. Even the effect of local disturbances of the tension through notching was investigated with test bars, but no endurance tests of complete structural parts have yet been published.

The results of endurance tests of the material in the form of test bars can be applied to the material actually

incorporated in the structures only when the stresses in the structures, including the local increments, are known. The extraordinary effect of the great local stresses is shown by the endurance tests of airplane parts described in this report, which were made with wooden spars and also with various metal spars. The results obtained for wooden spars agree surprisingly well with the expectations, there being no impairment through stress concentrations. The metal spars, on the contrary, show very unfavorable use of the material. This does not signify that they are not dynamically strong enough. It is obvious, however, that the metal parts exhibit a very poor ratio of dynamic strength to static strength. Of special interest are the results obtained with four spars for the same wing and the same static loads in comparative tests. Of these, one was of wood, one of elektron and two of high-tensile steel.

The present report describes the methods of testing and evaluation and gives the results of the first tests, in which complete structural members, particularly spars, were used. After the tests had shown the importance of the dynamic investigation of airplane parts, systematic tests were instituted for the purpose of determining the dynamic strength of various riveted transitional connections.

II. GENERAL PLAN FOR THE ENDURANCE TESTS

1. Dynamic Tests with Complete Structural Parts under Superposed Static Loading

The distribution of the loads, as assumed in the static calculation of an airplane, is specified in the "Load Assumptions." This is determined, for the wing, from the aerodynamic forces in the different conditions of flight, which forces are accurately enough known from aerodynamic measurements and tests. In static loading tests, these loads are increased in stages, first to the safe load and then up to the breaking load.

On the other hand, with dynamic loading tests of airplane structural components, the following questions call for answers.

1. How are the dynamic loads distributed?

2. How great a load should be used for the first dynamic test with a structural component?

3. To what superposed (basic) static load shall the structural component be subjected?

4. How can the endurance strength be determined, i.e., the load factor at which the stresses are still so small that the part can withstand any number of load reversals.

Questions 1 to 3 are relatively easy to answer for the dynamic strength tests of simple parts. For example, a Cardanic spar-strut fitting is stressed only in the direction of the strut and the load is varied only between two limits, the distance of which from the point of zero load can be more accurately determined in each individual case. As the limiting cases, one can first make a simple alternating-load test and then, in a second test, so choose the preliminary tension that the load will vary from zero to a maximum value (the original strength).

For the biplane struts investigated in this report, the problems of the dynamic load assumptions and load increments are very difficult.

Regarding question 1.- The dynamic stresses may be produced:

a) by exciting the natural vibrations of the spars (by shocks in taxying or by gusts),

b) by temporary fairly high additional loads (gusts).

The load distribution according to a) is easily obtained by mounting the spar on the test stand corresponding to its installation on an airplane and then setting up its natural vibrations. The load distribution according to b) is but little known and, since it differs in any case from the load distribution a, it is difficult to reproduce in the vibration test. Within certain limits, deviations from a may be effected by attaching suitably distributed masses to the spar. In the previous experiments with whole spars, the natural vibration of the spar was utilized for its dynamic loading, no special masses being attached. The unavoidable masses of the covibrating guides and suspension devices for the static superposed loading correspond approximately to the masses of the interior wing structure,

which are also securely attached to the spar in the complete wing.

Regarding question 2.- The magnitude of the dynamic stresses of the spar due to natural vibrations is characterized by the amplitude a at the tip of the spar. For the first loading stage of the dynamic tests with the investigated spars, the practical amplitude a at the spar tip was obtained from the experiments with the first spar of this series. According to a preliminary test with a = 3.2 cm (1.26 in.) and according to the alternating stresses measured, it was fixed for this spar at a = 5.9 cm (2.32 in.), at which the maximum dynamic stress, without considering the stress concentrations, was $\pm$ 12 kg/mm^2 ($\pm$ 17,068 lb./sq.in.) for a tensile strength of 120 kg/mm^2 (170,680 lb./sq.in.) of the material. It was assumed that no break could occur at alternating stresses of only 10 per cent of the tensile strength. The amplitude was to be increased after 2×10^6 load reversals, but rupture occurred after only 0.44×10^6 load reversals. Hence in the succeeding spars of like static strength, the amplitude at the first loading stage was fixed at about 2.5 cm (0.98 in.). In the first loading stage all the spars withstood 2×10^6 load reversals, and the amplitude was then increased.

Regarding question 3.- The superposed or basic static load corresponded to the load factor $n_A = 1.25$ and was therefore a little less favorable than in cruising flight.

Regarding question 4.- If the fatigue test of a sample bar is begun with a sufficiently small alternating load, if this load is gradually increased by stages, and if the bar is subjected, in every loading stage, to the critical reversal number, under a certain alternating load, up to fatigue fracture, the endurance strength of the material is not determined. The endurance strength of the material is increased by slowly increasing the alternating load. This method of increasing the load by stages was nevertheless employed in the dynamic spar tests, since a very great number of spars of like design would have been necessary for a determination of the actual endurance strength, and the unavoidable deviations of the individual spars would have concealed the effect of the improvement in the endurance strength of the material. Moreover the alternating stresses experienced by a spar in an airplane are so irregular that the comparison of these alternating stresses with the endurance strength of the material is not free from objection.

2. Superposed Static Tests

For determining the elastic characteristics of the spars, static tests were made before the dynamic tests. (Cf. IV, 2, c.) The load was increased to the requisite safe load, since the spars, even on an airplane in flight, are subjected to this static stress.

3. Dynamic Tests with Pieces of Broken Spars

In the dynamic tests the spars broke in the vicinity of the steel fitting, where the maximum bending moments occurred and the cross-sectional transitions had a dynamically detrimental effect. Since the break was limited to one place, loading tests could be made with the remaining pieces. In these tests there was no object in producing a combination of dynamic load and superposed static load corresponding to that on an airplane in flight. These pieces of spar were supported at two points and subjected to simple alternating stresses by the excitation of natural vibrations. Only in one case was a superposed static load applied in such a way that the stresses alternated over the entire length of the spar from zero to a maximum value.

III. EXPERIMENTAL APPARATUS

1. Mounting the Test Spar

The spars (upper wing of a braced biplane) were mounted corresponding to their position in an airplane on its back. (Figs. 7 and 8.) The end fitting of the spar was fastened to a heavy iron test frame of about 10,000 kg (about 22,000 lb.). The bracing cable, running, in the inverted position of the airplane, obliquely upward to the fuselage was replaced by a pendulum support running obliquely downward (to the right in Figure 7). This rested on a rigid wooden support anchored in the floor of the laboratory. The support of the spar was therefore very rigid. It was found that the more rigid the support, the better the vibration test proceeded, i.e., without beats and without noise. Original attempts to use rubber pads under the support utterly failed. The spar supports are also quite rigid on an airplane.

Vibration tests can be made on an elastic stand only with the whole airplane or with symmetrical parts. The only disadvantage of a rigid support lies in the fact that considerable energy is transmitted to the foundation, thus rendering impossible the measurement of the energy absorbed by the spar itself in the different stages of the test. The spar was guided by hinged parallelograms (figs. 16 and 33), so that it could not tip, buckle or vibrate sidewise.

2. The Unbalance

The natural vibrations of the spar were generated by means of a revolving unbalanced weight or "unbalance." The double unbalance, which was clamped to the spar, is shown in Figure 1*. The housing consisted of the ground plate G, the side walls W and a cover. This housing contained the driving gear Z and the two unbalance gears U_1 and U_2. The wheel Z was driven by the flexible shaft B through the coupling K. In order to free the latter from bending moments, the support S was rigidly attached to the housing. The wheel Z engaged U_2. The wheel U_1 was driven either by U_2 or by Z, according to the position of the adjustable bearing L_1. The bearing L_2 was fixed. To the unbalance wheels U_1 and U_2 were attached lead masses M_1 and M_2, which made the wheel unbalanced. The protecting net around the unbalance is not shown in the photograph.

In the spar tests the wheel U_1 was driven by U_2 (counter-rotation). The masses M_1 and M_2 were symmetrically arranged. In the test, therefore, only the vertical forces acted periodically on the spar. These double unbalances were too heavy and too broad for two spars, so that the single unbalance shown in Figure 8 was used, the all-sided excitation of which, did no harm when suitably applied near the end support. The unbalance was driven, through a flexible shaft, by an adjustable direct-current motor or by an alternating-current motor with an intermediate adjustable friction wheel. The characteristics of the various driving mechanisms are described in Section V.

---

* For the various uses of double unbalances, see Späht, V.D.I., 1930. Double unbalances are also used in the D.V.L. for investigating the vibration characteristics of whole airplanes.

Figure 9 shows a piece of spar as a beam on two supports and a pendulum support with unbalance near it. The lead masses screwed to the spar reduce the natural vibration number.

3. Test Wedges, Optograph, Tachometer, Tachograph, Scratch Instruments

a) Test wedges

The test wedges served for direct measurement of the vibration amplitude. Their mode of operation is shown in Figure 2. The smaller the amplitude at the measuring point, the smaller the wedge angle chosen. Figures 6 and 7 show the distribution of the twelve test wedges along the spar, whereby the wedge angle was adapted to the amplitudes. With the smallest of the wedge angles here used, amplitudes of only 0.1 mm (0.004 in.) could be easily read. The bending lines obtained with the aid of the test wedges were very accurate and no troublesome calculations were found necessary.

b) Optograph

The time rate of the vibrations can be accurately recorded by the optograph*. Figure 3 compares the flexural or bending lines in vibrations, as measured by the test wedges and by the optograph. The agreement is good.

c) Tachometer and tachograph

The frequency of the spar vibrating in resonance agreed with the revolution speed of the unbalance. The latter was measured by a tachometer which was connected with the unbalance by a string drive. (Fig. 7.) The number of load reversals could be read on a 1:20 counting mechanism which was applied to the motor. In a few tests the revolution speed was recorded by a D.V.L. tachograph. (Fig. 30.)

d) Scratch instrument

The alternating stresses were measured in a few in-

---

*Hans Georg Küssner, "Optisch-photographische Formänderungsmessungen." D.V.L. Report 194, Z.F.M., Vol. 21 (1930) pp. 433-440 and D.V.L. Yearbook 1931, pp. 227-234. For translation see N.A.C.A., T.M. No. 610.

stances with the aid of scratch instruments, for the checking of the stresses calculated from the measured vibration bending lines. (Cf. IV, 2, a and b.)

4. Superposed Static Load

a) Elastic suspension

In the superposed static loading of the spars in the vibration test, the weights were suspended on soft rubber shock-absorption cords. (Figs. 5a and 7.) A hardwood block provided with small guide strips was placed on the spar. Through this block passed a screw bolt with a nut on each end which clamped the cord against the block. The rubber cord carried a pulley, through which passed the pin of a clevis, which, in turn, carried the weight. The pulley was essential, because the two parts of the cord stretched differently during the test. Previous methods of suspension led to early breaks in the cord. (Figs. 2 and 38.)

The best shock-absorbing system was determined from static and dynamic tests. For heavy loads, fabric-covered rubber cords of 17 mm (0.67 in.) diameter are now used. The number of cords should be such that each cord will carry a load of 50 to 60 kg (110 to 132 lb.). For this diameter of the cord, the best results were obtained with a preliminary load of 65 kg (143 lb.). The load-elongation diagram (fig. 4) shows that, with a new rubber cord, the elongation was the greatest for preliminary static loads of 50 to 65 kg. The rubber cord was somewhat less elastic after a long vibration test, as shown by the dash line in Figure 4. It should be as long as possible. The tests showed that a length of 60 cm (about 2 ft.), as measured in the unstretched condition, was adequate. The preliminarily loaded cord then had a length of l = about 85 cm (33.5 in.). The elastic constant for the new cord stretched with a preliminary load of 65 kg (143 lb.); then became $c = 1.2$ kg cm^{-1} and increased in the endurance test with several million load reversals to c = about 1.7 kg cm^{-1}. This elastic constant remained practically unchanged for a travel of $\pm$ 6 cm (2.36 in.). Greater travels did not occur in the vibration tests. For light loads, fabric-covered rubber cords of 5 mm (0.2 in.) were used, the number of parts being such that each part carried a load of about 4 kg (8.8 lb.).

b) The motions of the preliminary loads

Let the suspension point H of the mass M (Figs. 5a and 5b) undergo a harmonic vibration of the rapidity $\nu(s^{-1})$. Let the distance of the suspension point from the zero point at the instant t be d sin νt. Let s denote the deflection of the mass M at the instant t. Let the effective elastic constant be $c(kg\ cm^{-1})$. Then the vibration equation for the elastically suspended mass M, disregarding the reaction on the vibration of the suspension point, the damping and the masses of the suspension cords, is

$$M \frac{d^2 s}{dt^2} - c[d \sin (\nu t) - s] = 0$$

The general solution of this differential equation reads

$$s = A \sin \nu' t + B \cos \nu' t + r \sin \nu t$$

Two differentiations of s and introduction into the differential equation yield the coefficients

$$\nu' = \sqrt{\frac{c}{M}} \text{ and } r = \frac{d}{1 - \frac{M}{c} \nu^2}$$

If the observation is begun at the instant when both H and M are at rest, then, with s = 0 for t = 0, B = 0 and consequently

$$s = A \sin \sqrt{\frac{c}{M}}\, t + \frac{d}{1 - \frac{M}{c} \nu^2} \sin \nu t$$

Accordingly two vibrations may be superposed whose rapidities $\nu' = \sqrt{\frac{c}{M}}$ (natural vibration of the elastically supported mass) and ν are widely separated. Their ratio is approximately

$$\frac{\nu}{\nu'} = \frac{100}{\sqrt{\frac{1.7 \times 981}{65}}} = 20$$

The coefficient A of the first slow vibration is determined as follows for the endurance vibration test, in which a definite periodic state of vibration must develop. It is assumed that the vibration ν' is completely damped out at $t = 0$. For this time we then have

$$\frac{ds}{dt} = A\nu' + \frac{d\,\nu}{1 - \frac{M}{c}\,\nu^2} = v = \frac{d\,\nu}{1 - \frac{M}{c}\,\nu^2}$$

and hence $A = 0$. The vibration of the mass M in the endurance test is then

$$s = \frac{d}{1 - \frac{M}{c}\,\nu^2} \sin \nu t$$

and half the amplitude is

$$s_{max} = \frac{d}{1 - \frac{M}{c}\,\nu^2}$$

For the elastic constants chosen in the tests

$$\frac{M}{c} = \frac{65}{1.7 \times 981} = 0.039 \ (s^2)$$

and the rapidity occurring in the tests

$$\nu = 100 \ (s^{-1})$$

we obtain

$$\frac{s_{max}}{d} = \frac{1}{1 - \frac{M}{c}\,\nu^2} = -\frac{1}{390}$$

For a very great vibration amplitude of d = about 4 cm (1.57 in.), the deflection of the mass is therefore only $s_{max} = 0.01$ cm (0.004 in.). In the tests therefore no motions of the superposed static loads could be established.

c) The additional dynamic stresses due to the superposed load

As already shown and confirmed by tests, the motions of the masses of the superposed static load were negligibly small. The dynamic additional loads of the superposed static load were affected only by the deflections of the point of suspension and by the elastic constant and were therefore easily calculated. The additional loads could be reduced in proportion as the elastic cord was softer (and therefore longer). Despite the fact that the length of the cord, 85 cm (33.5 in.) for the spar tests in the condition of superposed load was limited by the height of the test apparatus, the additional forces in the tests were very small. Figure 6 compares the superposed static load and the additional dynamic load for the wooden spar II for an amplitude of 4.4 cm (1.73 in.), d = 2.2 cm (0.866 in.). The inertia forces and the additional forces, however, were opposed. In general the additional forces could be disregarded. Moreover the additional forces, due to the elastic suspension of the superposed load, could be eliminated by additional masses, firmly bound to the vibrating suspension points H. As will be shown, the inertia force of a vibrating additional mass at the reversal point of the motion was

$$P_{x1} = - m_x d_x \nu^2$$

as compared with the additional elastic force

$$P_{x2} = d_x c_x$$

The forces cancel out, when

$$P_{x1} + P_{x2} = 0$$

so that

$$d_x c_x - m_x d_x \nu^2 = 0$$

or

$$\underline{m_x = \frac{c_x}{\nu^2}}$$

d) Advantages of the freely vibrating superposed load

If instead of suspending weights, the force is generated by anchoring the cords to the floor, the additional dynamic forces will remain the same. It is difficult, however, to equalize the tension at the numerous loading points (11 in spar II). Every cord would require a dynamometer to verify the preliminary tension, because the rubber cords continually stretched in the endurance tests. The suspension of a constant superposed load on a rubber cord is therefore simpler and more accurate than anchoring the cord to the floor.

5. Excitation of Natural Vibrations by a Revolving Unbalance

a) The 16,000 kg (35,274 lb.) test apparatus

Figure 10 shows an endurance-test device, which was developed from the device for testing spars. Here the structural part to be tested did not vibrate of itself, but was periodically stressed by a loading lever D oscillating in its natural-vibration number. This lever, consisting of two channel irons, was so mounted statically determinate on two vertical supports A and B, that there was a long overhang (toward the right in the picture) of 90 per cent of the whole length. A double unbalance G was securely bolted to the free end of the overhang. This unbalance was driven by a direct-current motor through a flexible shaft K. Moreover, for the test in question, a superposed static load H was suspended by rubber cords from the overhanging end. The lever D was secured against lateral tipping, turning and oscillating by two hinged parallelograms E which are only partially visible in the picture. The horizontal rod C held the whole apparatus in place longitudinally. The single vertical bearing A (at the left in the picture) was provided with a round steel rod as a pendulum support. (Fig. 11.) This rod was supported between transverse knife-edge bearings, roller bearings having proved unsatisfactory. The test rod was made so long that elongation measurements could be made on it with scratch instruments of 20 cm (7.87 in.) gage length. In the test, due to the superposed static load, it was always stressed in compression. In the original form, the device was provided with a tension member at the bearing A. Fatigue breaks often occurred at the junction of the tension

rod. The part to be tested (in this case a connecting rod) was mounted on the bearing B. The connecting rod formed a pendulum support between central knife-edge bearings. The supports A and B were firmly anchored to the base L over a heavy iron rail.

The lever D was now set in vibration by the revolving unbalance, whereby the bearing force at B was utilized for the loading test of the connecting rod. The amplitude line of the lever D was determined by the measuring wedge. In the experiment shown in Figure 10, the load alternated between 0 and 16,000 kg (35,274 lb.) with a frequency of 560 times per minute. At this stage the device had withstood about 10^7 load reversals. Its vibration number could be changed somewhat by additional weights F on the overhanging end.

Figure 12 shows the endurance-test apparatus for 8,000 kg (17,637 lb.) load. In this case the structural part to be tested was mounted at the bearing A. Figure 13 shows further details. With a suitable form of the mountings A and B and the use of various superposed static loads, alternating loads with any desired zero point could be applied to the 16,000 kg (35,274 lb.) apparatus. The results obtained with this apparatus are given under IV, 2, b.

b) The vibrating mechanism

The application of the vibrating mechanism is shown in Figure 14. A spherically-headed bolt was firmly clamped in its spherical socket K by tightening the screw cap. In tramsverse vibrations of the strut joined to this bolt, alternating bending moments develop in the shaft of the bolt, which, with sufficient amplitude, necessarily cause fatigue breaks. The durability of the bolt under this stress had to be determined by experiment. The fitting A was screwed, with the bolt, to the wooden beam B, which was provided with an unbalance e. A substitute iron rod D, instead of the strut, was screwed on the thread of the bolt. The unbalance was driven by the direct-current motor E through a flexible shaft, and its revolution speed was so adjusted that it was in resonance with the natural vibration number of the rod D. The vibration bending line of the rod D was determined with measuring wedges. The alternating fixed-end moments can be very accurately calculated from the bending line, the rod masses and the frequency. Figure 14 also shows the superposed load, applied through a rubber

cord, which exerted a fixed-end moment, so that, in the vibration test, the moment alternated between zero and a maximum moment. The static moment might, of course, be applied in another direction and magnitude.

Figure 15 shows the results of the tests with spherical-headed bolts. The left-hand break (a) occurred on an airplane. Almost the entire cross section shows the relatively smooth fatigue break, while only a narrow strip through the middle has the rough appearance of the static break. The middle specimen (b) shows a break produced in the vibration test without superposed loading, i.e., with a fixed-end moment, which alternated between equal maximum positive and negative values. This specimen also shows the symmetrical fatigue break and the static final break in the form of a narrow strip through the middle. The last specimen (c) shows a break produced in the vibration test for the original strength with superposed static load. The final static break did not pass through the center, but along a chord far to one side. Breaks a to c indicate that the bolt on the airplane was broken by simple strut vibrations without superposed static stresses.

IV. INTERPRETATION OF THE RESULTS

1. Calculation of the Dynamic Stresses Resulting from the Inertia Forces of the Spar

The inertia force P_x of a vibrating spar section at the point x with the mass m_x is

$$P_x = m_x b_x \text{ in kg}$$

in which the acceleration is b_x (m/s^2), for the calculation of which the following values serve:

υ = rapidity = $\frac{\omega \, 2 \, \pi}{60}$ per second, where ω is the measured number of vibrations per minute;

a_x = maximum value of measured amplitude at the point x in meters. (Total amplitude a_x = sum of deflections in both directions.)

The distance (s)-time (t) equation of the vibrating masses m_x reads

$$s_x = \frac{a_x}{2} \sin \nu t$$

The velocity is then

$$v_x = \frac{ds_x}{dt} = \frac{a_x}{2} \nu \cos \nu t$$

and the acceleration

$$b_x = \frac{d^2 s_x}{dt^2} = - \nu^2 \frac{a_x}{2} \sin \nu t$$

The maximum acceleration occurs at the reversal point of the motion, where

$$v_x = \frac{a_x}{2} \nu \cos \nu t = 0$$

and hence, with

$$\cos \nu t = 0 \text{ and}$$
$$\sin \nu t = 1,$$

we have

$$b_{x\ max} = - \nu^2 \frac{a_x}{2}$$

The maximum inertia force is therefore

$$\boxed{P_x = - m_x \nu^2 \frac{a_x}{2}}$$

or

$$P_x = - 0.00548\ a_x\ m_x\ \omega^2$$

In all these vibration tests, the mass distribution, the amplitude line and the rapidity of the vibrating parts or of the vibrating load apparatus were determined and the dynamic loads calculated from them. A few examples of the method of determining the inertia force are given in Figures 18, 20, 24, 25, 32, 34 and 35. The dynamic bearing forces, bending moments, tensile forces and stresses were calculated

from the inertia forces by well-known methods.

Of course the masses of the parallel guides and of the unbalance had to be considered in connection with the mass distribution. Because of its great mass, it was advisable to install the unbalance near a support. The double unbalance weighed about 20 kg (44 lb.). This also had the advantage that the additional stresses from the centrifugal forces of the revolving unbalances were small (chiefly negligible). The centrifugal forces of the unbalance in the 16,000 kg test apparatus had to be taken into consideration, however, since they were exerted at the end of the long overhanging arm.

2. The Checks of the Dynamic Stress (Inertia-Force) Calculation

The above method is doubtless all right, but a check is often desired, especially when the mass distribution is less accurately known. The various checks, which have thus far been used in the tests, will now be briefly described.

a) Direct stress measurements with scratch instruments

The mounting of the steel spar I for static loading is shown in Figure 16. It was only slightly modified for the dynamic tests, as shown in Figure 17. Scratch instruments were mounted on both flanges of the overhanging arm at 50 cm (19.7 in.) from the supporting strut. These instruments recorded the elongation and the stresses during the vibration test. The tensometer could be used only in the vicinity of the support, where the vibration amplitude of the spar was small. Farther from the support the vibration amplitudes and consequently the accelerations of the instrument masses were greater, thus requiring excessively high clamping forces for the instrument. Figure 18b shows the course of the accelerations throughout the length of the spar. In the turning point of the motion at the tip of the spar, the acceleration was about 23 times the acceleration due to gravity and was proportional to the amplitudes throughout the length of the spar. The maximum acceleration at the fixation points of the scratch instruments was 5.5g. Figure 19 shows the record of a test. It shows the 125-fold magnification of the alternating elongations of the lower flange for an amplitude of 36 mm (1.42 in.) at the tip of the spar. On the assumption of a Young's modulus of $E = 2.2 \times 10^6$ kg/cm^2, the alternating stress $\sigma_w = \pm 410$ kg/cm^2 ($\pm 5,832$ lb./sq.in.). When reduced to the maximum amplitude a_{max} =

4.44 cm (1.75 in.) investigated in Figure 18, the experimental alternating stress becomes $\sigma_{wv} = \pm$ 505 kg/cm^2 ($\pm$ 7.183 lb./sq.in.) as compared with the calculated alternating stress of σ_{wr} = 530 kg/cm^2 ($\pm$ 7,538 lb./sq.in.) in Figure 18. The 5 per cent deviation is small enough, but the angular elongation record with superposed secondary vibrations in Figure 19 is less satisfactory. The disturbances are largely ascribable to the poor fixation and the relatively high instrument accelerations of $\pm$ 5.5g.

b) Scratch-instrument measurements of the dynamic reactions of the supports

The reactions of the supports obtained from the calculated inertia forces can be checked by stress measurements on the supports. The measurements are simpler, because the instruments undergo only very small alternating accelerations at the supports. The supports must, of course, be suitably constructed. Hence these measurements were omitted in the spar tests. The test of the connecting rod was made with the 16,000 kg (35,274 lb.) apparatus. (Figs. 10 and 11.) There was perfect agreement between the directly measured stresses and those calculated from the inertia forces. The calculation of the latter is illustrated by Figure 20. This figure is especially intended to show the distribution of the masses and the bending line of the lever. The lever turned principally about the very rigid pressure bearing B, while the less rigid bearing A (with tensile forces in the supporting structure) yielded more. Fifty per cent of the end amplitude of the overhanging arm was due to the turning of the lever, while the rest of the end amplitude was due to the bending of the lever itself. A few selected records are shown in Figures 21 and 22.

The records in Figure 21 were made for a load of the connecting rod of $\pm$ 4,000 kg ($\pm$ 8,818 lb.) and a superposed static load of -4,000 kg.

The two records were made simultaneously by two scratch instruments (D2 and D22) clamped to the opposite sides of the test bar. The difference in the amplitudes of D2 and D22 is due to the bending stresses caused by the support not being exactly centered. The interpretation of the diagrams, which are magnified 110 times, yielded the results given in Table I.

Table I. Endurance Test of a Connecting Rod

Instrument		Total amplitude	Half amplitude	Stress	Cross section F	Force P
D2	D22	mm × 10^{-2}	mm × 10^{-2}	kg/cm^2	cm^2	kg
19.5	12.2	15.85	7.93	1,010	7.07	7,127

Calculated P_r = 7,207

cm^2 × .155 = sq.in.
kg/cm^2 × 14.2235 = lb./sq.in.
mm × .03937 = in. kg × 2.20462 = lb.

The agreement of the calculated results (from the inertia forces) and the experimental results is exceptionally good. The straight lines in the records are zero lines, the position of which is nevertheless arbitrary. The records are quite regular wave forms. The amplitudes of the high-frequency secondary vibrations are insignificant.

Figure 22 is a hundredfold enlargement of a record of a connecting-rod test with an alternating load of about ± 6,000 kg (± 13,228 lb.) and a superposed load of about -6,000 kg in the connecting rod. With a hundredfold enlargement, an amplitude of 1 mm (0.04 in.) corresponds to a force of 765 kg (1,686 lb.) in the test bar. In addition to the vibrational stresses the record also shows the following basic elongation lines.

a) Indication of the instrument for the stationary machine with superposed static load,

b) Indication of the instrument for the stationary machine without superposed static load.

In the following example the vibration record is evaluated and compared with the calculated inertia forces.

Test

6.65 mm half-amplitude (0.262 in.) corresponds to P_d = ± 5,100 kg (±11,244 lb.)
7.70 mm static displacement (0.303 in.) corresponds to P_s = - 5,860 kg (-12,919 lb.)
Total P = - 10,960 or -760 kg
(-24,163 lb.) (- 1,676 lb.)

Calculation

Force in test bar from inertia forces $P_m = \pm 5{,}479$ kg ($\pm 12{,}079$ lb.)

Force in test bar from superposed static load $P = -5{,}850$ kg ($-12{,}897$ lb.)

Total $P = -11{,}329$ or -371 kg ($-24{,}976$ lb.) (-818 lb.)

The vibrations are not very pronounced, so that the result of the evaluation is not so good as for Figure 21. The most important thing in Figure 22 is the experimental proof of the shifting of the zero line of the loading by the superposed static load.

c) Comparison of the measured bending line

with the bending line calculated from:

α) The inertia forces and the course of the experimentally obtained bending stiffnesses EJ along the bar,

β) The inertia forces and the influence coefficients for the spar deflections, as determined in the static tests.

α) If the inertia forces of the vibrating bar (from the vibration bending line, masses and frequency) and the bending stiffness EJ along the bar are known, the bending line can then be calculated by well-known static methods (graphically according to Mohr; mathematically according to Müller-Breslau). If the calculated bending line agrees well with the measured, it is a proof of the correctness of the determination of the dynamic stresses, into which errors may creep, e.g., through false assumptions of the mass distribution. The course of the bending stiffness EJ can be calculated quite accurately for metal spars. Experimental determination is desirable, however, for wooden parts, because of the unknown Young's modulus which varies along the spar. Figure 16 is a photograph of a static test. The deflections are read with the leveling instruments on the measuring strips, and the flange elongations are read with a Huggenberg tensometer. From the measured bending lines we obtain the EJ curves by two differentiations, which however yield relatively inaccurate results. Very accurate EJ curves are obtained from the elongation measurements

$$EJ = \frac{M\,(d_o + d_u)}{\epsilon_u - \epsilon_o} \text{ in kg/cm}^2$$

when

M, the bending moment in kg cm in the tested cross section,

ϵ_u, the compression or elongation of the lower flange as measured at the distance d_u (cm) from the zero line,

ϵ_o, the elongation or compression of the upper flange as measured at the distance d_o (cm) from the zero line.

The determination of the EJ values and the comparison of the measured and calculated vibration bending line for the wooden spar I are shown in Figure 24. The order of the measurements is shown in Figure 23. The measured strains (calculated for stress with E = 146,000 kg/cm^2 (2,076,631 lb./sq.in.) are compared with the purely mathematical values in Figure 24b. The EJ values calculated from the elongations are plotted in Figure 24c along with the inertia moments J.

$$E = EJ_{exp.}/J_{calc.} = 146{,}000 \text{ kg/cm}^2$$

The deviations of Young's modulus from this mean value in the individual cross sections are apparent from the plotting along the spar.

In Figure 24d to 24f are plotted the mass distribution d for the dynamic test, the vibration bending line e and the therefrom calculated inertia forces f for the vibration number ω = 1,120/min. From these inertia forces and the experimental bending stiffnesses EJ, the bending line is again calculated according to the method of the "elastic weights" and compared in Figure 24g with the directly measured bending line. The calculated line shows only about 5 per cent greater deflections. Otherwise the two lines agree very well. The 5 per cent discrepancy is attributable to the fact that the load acted for a long time in the determination of the EJ values in the static test, whereby the distortions were greater than in very short loadings, as in the vibration test.

β) The method described under α requires a greater number of tensometers. It also has the disadvantage that the shearing distortions are disregarded in the recalculation of the bending line. Another simple method was therefore adopted for the wooden spar II. The bending lines of the spar were measured at 21 points under a static load of 150 kg (330 lb.), which was successively applied to 21 cross sections of the spar. The deflection at the point i on the spar resulting from a unit load at the cross section k is designated by δ_{ik}. The influence coefficients were obtained from the test with a shifting single load. The bending line can now be calculated from the inertia forces and influence coefficients.

The inertia force is calculated for the wooden spar II in Figure 25, while the influence coefficients δ_{ik} are given in Table II. (See page 35.) The vibration bending line, as recalculated from the inertia forces and influence coefficients, is compared in Figure 26 with the directly measured vibration bending line. The agreement of the two lines is very good. Contrary to expectation, the calculated deflections are smaller than the measured ones. This discrepancy is apparently due to the buckling effect, which is not contained in the influence coefficients. The method of checking the calculated inertia forces by recalculating the vibration bending line with the aid of the influence numbers δ_{ik}, was also used successfully for vibrating spars in the wing structure.

The comparison of the calculated with the measured vibration bending line of a two-spar wing in Figure 27 shows satisfactory agreement, so that the approximately calculated mass distribution of the wing is sufficiently exact and can therefore be used with satisfactory accuracy for every other dynamic verification. Moreover, the agreement of measurement and calculation shows that the static influence coefficients δ_{ik} can be introduced even into dynamic calculations with adequate accuracy.

V. EXECUTION OF THE TESTS

1. Driving the Unbalance

The execution of the test depends very largely on the method of driving the unbalance.

a) Alternating-current motor with adjustable friction drive

This method is well adapted for determining resonance curves, because it is possible to adjust the driving gear so as to maintain any exciting frequency. If, in an endurance test, the friction drive is so adjusted as to produce resonance between the revolution speed of the unbalance and the natural vibration rapidity of the structural part, the test then requires no further special attention, because no cessation of the resonance is to be feared so long as the spar does not begin to break and the bearing conditions do not materially change.

b) Direct-current motor with Leonard control

By this method any desired revolution speed can be easily obtained without the use of the friction drive which increases the difficulty of setting up the testing apparatus.

c) Adjustable direct-current motor

The adjustment is made either by the upward adjustment of a motor of smaller revolution speed than the resonance rapidity by weakening the field, or by the downward adjustment of a high-speed motor by weakening the armature current. The speed of the direct-current motor depends on the power absorption of the structural part and on the fluctuations in the voltage. Hence an endurance vibration test with direct-current drive requires close attention. By warming or by voltage fluctuations, the motor is apt to lose its accurately adjusted resonance and begin to race.

2. The Phenomenon of Breaking

The sensitiveness of the adjustable direct-current motor is very favorable for the execution of the test at the beginning of the dynamic break. The change in the power absorption of the vibrating part by the dynamic break is so great that the incipient break is immediately evidenced by the irregular course of the vibrations and the racing of the motor. If these signs of a break occur, the test is immediately interrupted and the break discovered in its initial stage. Figures 28 and 37 show breaks of this character, which were discovered by the timely interruption of the tests. In a resumption of the test, the break advanced

about a centimeter during about 11,000 load reversals. The break was then completed in about 300 more load reversals. Figure 29 shows, in the evaluation of an amplitude record made with an optograph, that no regular vibration could be obtained after a dynamic break, due to the constantly changing power absorption and stiffness of the spar. The amplitude increases as the break progresses, while the natural frequency decreases. The revolution speed diminishes immediately before the complete break, due to the great energy absorption for the work of breaking. As soon as the break is completed, the engine begins to race. A section of the revolution-speed record for the steel spar I is shown in Figure 30.

3. Discovery of a Dynamic Break

This is often very difficult. For metal spars with closed sections, the following method is recommended for finding the break. Before the beginning of the vibration test, the inside of the spar is smeared with thick dark oil, while the outside of the spar is kept free from oil. The great accelerations occurring in connection with the vibrations force the oil through even very fine cracks, so that it appears as a dark line on the outside of the spar. Where rivets are used, this method will show whether they are tight, because loose rivets would let the oil through.

VI. TEST RESULTS

1. Steel Spar I (welded)

This spar was made of thin Swedish chrome-nickel steel plates of 125 kg/mm^2 (177,794 lb./sq.in.) tensile strength forming a box with point-welded joints. (Fig. 31.) With respect to the vibration strength, the flange material was very unfavorably affected by the welds between flange and web, which lay in a highly stressed part of the flange. Moreover, at this point of weakness, local stresses were produced by the transmission of forces at the junction points. Two tests were made.

a) Entire spar

The mass distribution, bending line, inertia forces, dynamic stresses and superposed static stresses due to the load factors $n_A = 1.3$ are represented in Figure 18. The

most important numerical values obtained during the test are given in Table III.

The break in the lower flange of the inner bay near the strut fitting proceeded, as shown in Figure 31, from the middle of the weld point a to the middle of the opposite weld point. A piece of the strut fitting was torn off at the point of rupture a. The rupture of the web occurred after that of the flange. It is worthy of note that the break occurred at the first weld which joined the strut fitting to the flange and which then gave rise to great stresses. The flange breaking stresses were therefore quite small, despite the small number of breaking-load reversals, as shown in Table III.

b) Inner piece without overhang

The mounting of the inner piece (which was unharmed in the first test) as a beam on two supports, is shown in Figure 32. Since the stresses at the breaking point in the first test alternated between -2.8 and 19.8 kg/mm^2 (28,163 lb./sq.in.) and therefore corresponded closely to the stresses of "original strength" (alternations between zero and a maximum value), the inner piece was tested with respect to its "original strength." Figure 32 shows the calculation of the superposed static and dynamic stresses, which, through an appropriate choice of the superposed static load, fluctuated between zero and a maximum value. The principal numerical test data are given in Table IV. The beginning of the break is visible in Figure 28. The break started at a weld, which, however, joined only the web and flange and was therefore not affected by the neighboring welds. Although the material had a strength of 125 kg/mm^2 (177,794 lb./sq.in.), the break occurred in the first vibration test after only 432,000 load reversals under the very small alternating stress of $\sigma_w = \pm$ 11.3 kg/mm^2 ($\pm$ 16,073 lb./sq.in.) and σ_s = 8.5 kg/mm^2 (12,090 lb./sq.in.) preliminary stress, and therefore at a total alternating stress of -2.8 to 19.8 kg/mm^2 (-3,983 to 28,163 lb./sq.in.). In the second vibration test, the complete break occurred after 325,000 further load reversals with an alternating stress of 0 to 19 kg/mm^2 (27,025 lb./sq.in.) (pure original stress). The two tests therefore agreed well. The attained original breaking stress σ_u of the spar, at the given tensile strength σ_z of the flange material σ_z = 125 kg/mm^2 (177,794 lb./sq.in.), was only

$$\sigma_u = \frac{19\ \sigma_z}{125} \doteq \text{(about) } 0.15\ \sigma_z$$

2. Steel Spar II (riveted)

This spar was made of the same thin Swedish chrome-nickel steel plates of 125 kg/mm^2 tensile strength as spar I. The flange and web and the fittings were joined by rivets. Two vibration tests were also made with this spar.

a) Entire spar. The test arrangement is shown diagrammatically in Figure 34.

b) Overhang as beam on two supports. The overhanging part was not harmed at all in the first test. It was also provided at the tip with a pin bearing and mounted as a beam on statically determinate supports. Since the short piece of spar had too high a natural vibration number for the test, it was weighted with masses of lead securely attached by screws. The installation corresponds to Figure 8 and the test results are plotted in Figure 35. The principal experimental results for the entire spar and for the overhang are given in Table V.

The breaking cross sections lay, in both tests, at the point of the greatest alternation of tensile and compressive stresses. The shifting of the stress picture by the superposed static load in the first test was not very great and is disregarded in the following discussion. The two tests agree well. The alternating breaking stresses were:

Test 1, $\sigma_w = \pm$ 15.4 kg/mm^2 ($\pm$21,904 lb./sq.in.) at 700,000 load reversals,

Test 2, $\sigma_w = \pm$ 16.0 kg/mm ($\pm$22,758 lb./sq.in.) at 58,000 load reversals

The endurance vibration strength was therefore still under

$$\sigma_D = \frac{15.4}{125}\ \sigma_z = 0.125\ \sigma_z$$

With respect to the cross-sectional transition, the riveting, etc., the spar was similarly built at both breaking cross sections. Hence the two breaks look alike, as shown in Figure 36. Under the continuous flange, a reinforcing plate began shortly before the row of rivets in which the

break occurred (first rivet row). The single rivet in the middle of the flange shows that the reinforcing plate continues toward the right. It terminates therefore at the left near the three rivets. Hence the break also runs through the rivet edges of the main section on the left. To the right of the rivets the main section was relieved by the reinforcement. To the left, on the contrary, unfavorable stresses were produced at the rivet holes in the continuous flange by the transmission of the stresses to the reinforcing strip. Figure 37 shows the break which developed equally in both directions from one of the three neighboring rivets.

For the following reasons, the first rivet row affords excellent places for the dynamic break and is the cause for the small alternating strength.

1. The reinforcing plate ends in a smooth section crosswise to the longitudinal corrugations and does not taper to a point. It ends in full width at the first row of three rivets. The succeeding rivets are placed at longer intervals and are staggered. The stress transmission from the continuous flange to the reinforcing plate therefore occurs chiefly in the first row of rivets. The first rivets are thus very greatly overstressed and there are very great stress concentrations in the vicinity of the rivet holes. The stresses in the continuous flanges concentrate, even without the force transmission through the rivets, due to the effect of the holes on the rivet-hole walls.

2. The arrangement of three rivets in one cross section is detrimental, due to the superposing of the stress concentrations.

3. The riveting is defective, due to the profile curvature at most of the riveting points. The flange surface is somewhat impaired by the pressure of the sharp rivet edges, so that notch effects are to be feared.

It is necessary to graduate the stress transmission by tapering the end of the plate and to avoid riveting in the outer fibers of the flange corrugations. It is sufficient to include the flange filling in the staggered riveting. The reinforcing plates must then taper out to two points.

3. Steel Lattice Spars

The spars described under a and b had plain webs. The diagonals of the lattice spars, on the contrary, were each attached to the flange with the aid of fittings. The flange material had a tensile strength of 75 kg/mm^2 (106,676 lb./sq.in.). One of the three spars tested was mounted for the vibration test with a superposed static load corresponding to $n_A = 1.3$. (Fig. 38.) Table VI gives the results of the four tests with the three spars, spar No. 2 having been repaired after the first break. Three forms of breaks occurred, as shown in Figure 39.

First form.- The breaks of spar 1, $2b_2$ and 3 were alike. Hence only the break of spar 1 is shown in Figure 39a. The break occurred in the first rivet row of an overlapped joint and is attributable to the same causes as in the case of the riveted steel spar II. (These plates were not originally present in the tested spars, but were riveted on, after the spars had been damaged in a static test. In doing this, there was no thought of using these spars for the dynamic tests.) Despite the similar appearance of the breaks, the breaking stresses differed greatly in the three cases:

Spar 1. $\pm$ 4.6 kg/mm^2 ($\pm$ 6,543 lb./sq.in.) after 2.29×10^6 load reversals,

Spar $2b_2$. $\pm$ 3.2 kg/mm^2 ($\pm$ 4,552 lb./sq.in.) after 1.88×10^6 load reversals (and 5.13×10^6 load reversals with smaller stresses),

Spar 3. $\pm$ 2.4 kg/mm^2 ($\pm$ 3,414 lb./sq.in.) after only 0.46×10^6 load reversals.

Second form.- The break of spar 2a (fig. 39b) began at the first rivet of a joint fitting. Great stresses naturally occur at the rivets of such a joint, but nevertheless the extremely small alternating breaking stress of 3.1 kg/mm^2 (4,409 lb./sq.in.) after only 2.94×10^6 load reversals was surprising.

Third form.- As shown in Figure 39c, the break of $2b_1$ proceeded from an injury (bulge) resulting from a previous test. It is the only break in all the steel-spar tests, which did not start at a rivet hole. At a high load-reversal number, the alternating breaking stress was 3 kg/mm^2

(4,267 lb./sq.in.). The ratio of the alternating strength σ_w to the tensile strength of the material σ_z varied between $\sigma_w = 0.032\ \sigma_z$ and $\sigma_w = 0.061\ \sigma_z$ and was therefore very poor.

4. Duralumin Lattice Spars

Two duralumin lattice spars, of the same type as the steel lattice spars, were tested for their vibration strength. Both broke, as shown in Figure 40, at the same point in the first rivet hole of a joint fitting (cf. fig. 39 b) and under the same stresses

$$\sigma_{stat} = + 3.8\ kg/mm^2;\ \sigma_{dyn} = \pm 1.8\ kg/mm^2$$

one after 2.8×10^6 and the other after 0.37×10^6 load reversals. The stresses attained are very small in comparison with the tensile strength of duralumin of about $\sigma_z = 40\ kg/mm^2$ (56,894 lb./sq.in.).

5. Wooden Spar I with Spruce Flanges

a) Source and type of spar

The spar investigated was taken from a biplane which in 1927 was subjected to a Case A breaking test, in which the front spar was not damaged. Before the beginning of the test in March, 1930, it was removed from the wing, which had been kept till then in a hangar of the D.V.L. without any special protection.

The wooden spar was of the standard box type. The flanges were made of spruce and the webs of birch plywood with diagonal direction of the grain. Plywood with the grain parallel and perpendicular to the spar axis was glued to the outside of both flanges.

b) Results of the vibration test

The test arrangement and results are shown in Figures 24 and 41. The test results are given in Table VII. In this test the amplitude was increased in four stages, until the break occurred. The stress variation along the spar for the lowest loading stage is represented in Figure 41. The spar broke after a total of 1.96×10^6 load reversals on the inner bay of the lower flange in the most highly

stressed cross section, at a point where the superposed static stresses were very small. The breaking cross section, which is very illuminating with regard to the dynamic breaking of a wooden spar, is clearly shown in Figure 42.

The break, beginning at a, has at first the characteristics of a smooth continuous break (as if cut with a saw) and gradually grows rougher to the other side of the spar and passes into the final static break. The same phenomenon is also exhibited in the outer plywood layer.

Before the break the amplitude was about 10 cm (3.94 in.) for the last dynamic loading stage $a_{max} = 11.4$ cm (4.49 in.). Shortly before the complete break, the amplitude fell to 8.5 cm (3.35 in.). This was due to the increasing energy absorption of the advancing break. Shortly before the beginning of the break, the flange stresses were:

Upper flange. $\sigma = -240$ kg/cm^2(-3,414 lb./sq.in.)(no break),
210 kg/cm^2 (2,987 lb./sq.in.)
Lower flange. $\sigma = 240$ kg/cm^2 (3,414 lb./sq.in.) (break).
-210 kg/cm^2(-2,987 lb./sq.in.)

c) Analysis of the results

Since it appears that the results agree extraordinarily well with the expectation based on the durability of the material, they will be described here in detail.

α) The durability σ_d of the material used.- The number of load reversals, which a piece of material can withstand without breaking, depends on the magnitude of the alternating stresses. According to recent tests of the alternating strength of wood, there is, with decreasing alternating stresses, a rapid and uniform increase in the number of load reversals which the wood can withstand without breaking. Only when a certain alternating stress, the durability, is not exceeded, will no break occur, even at a very high number of load reversals. The durability of a material has therefore certainly not been exceeded if the material has reached a certain critical number of load reversals. This number was fixed for spruce at $n = 2 \times 10^6$ by the material section of the D.V.L.*. The durability of the ma-

*O. Kraemer, "Dauerbiegeversuche mit Hölzern." D.V.L. Report 190. Luftfahrtforschung, Vol. 8 (1930), pp. 39-48, and 1930 D.V.L. Yearbook, pp. 411-420.

terial was already exceeded with the vibration strength σ_w = about $\pm$ 230 kg/cm² ($\pm$ 3,271 lb./sq.in.) attained in the vibration endurance test of the spar at n = 0.135 X 10^6 load reversals. The durability σ_d of the spar, according to the results obtained for spruce by the material division of the D.V.L., appeared to be about 20 per cent below the attained vibration strength $\sigma_w = \pm$ 230 kg/cm² ($\pm$ 3,271 lb./sq.in.) at $\sigma_d = \pm$ 190 kg/cm² ($\pm$ 2,702 lb./sq.in.).

β) The compressive strength σ_k of the flange material.- The materials were tested in four groups of ten samples each. The compression cubes, with the dimensions given in Figure 44, were cut from the spruce flanges as shown in Figure 43. The results of the compression tests are indicated in Figure 44. The samples of group 2, measuring 13.5 mm (0.53 in.) on an edge without plywood, yielded the highest mean value of $\sigma_k' = 439$ kg/cm² (6,244 lb./sq.in.). The strength of the samples of groups 3 and 4 is diminished by the plywood. Since, in the complete spar, the share of the plywood in the whole cross section of the flange is nearly the same as in the samples of group 3, the compressive strength $\sigma_k = 420$ kg/cm² (5,974 lb./sq.in.) will be taken as the basis for the further evaluations.

γ) The moisture content of the wood.- This was determined for two groups of flange plates of about 7 cm (2.76 in.) length both with and without plywood. In the drying oven both groups yielded a moisture content of 12 per cent which is regarded as normal.

δ) Expected and attained durability.- From α and β we obtain

$$\frac{\sigma_d}{\sigma_k} = \frac{190}{420} = 0.452$$

This agrees closely with the values of $\sigma_d / \sigma_k = 0.40$ to 0.45 obtained by Angstrom in bending spruce back and forth and with the values obtained by Kraemer, so that no impairment of the durability of the flanges resulted from the incorporation of the material in the box spar (disturbance of the stresses in the ribs and covering plates).

d) Summary of the results

With continuous gluing which does not injure the material it could be expected that the endurance of the entire structural part would agree with the material tests. Since, according to recent material investigations, the durability of spruce is about 45 per cent of its compressive strength, the results of the tests of the structural parts agree very well with the expectation. This agreement shows that the method used, which gave such unfavorable results for metal spars, is free from objections.

6. Wooden Spar II with Pine Flanges

The structure of this spar was similar to that of spar I. It was tested in the unused condition. Its structure is shown in Figure 6. The test results are given in Figure 25 and Table VIII.

VII. SUMMARY

Experimental apparatus and evaluation methods were developed and tried for the execution of vibration-strength tests with entire structural parts both with and without superposed static loading. Altogether ten metal spars and spar pieces and two wooden spars were subjected to vibration breaking tests. The wooden spars showed no diminution in the durability of the flanges as compared with that of the material used. The durability of the metal spars, on the contrary, was only a fraction of the durability of the material, due to local stress concentrations, which were a multiple of the mean stresses involved.

The good results obtained with wooden spars are attributable to the continuous cross-sectional transitions and force transmissions and to the glued joints which did not impair the material. The poor results of the metal spars were due to the detrimental stress concentrations at the abrupt cross-sectional transitions (fittings) in the first rivets or rivet rows and to the detrimental effects of the working of the material on its properties.

Further research is necessary to determine how much the dynamic strength of the metal spars can be improved by suitable constructive methods. Corresponding systematic researches are being instituted by the D.V.L.

Translated by Dwight M. Miner,
National Advisory Committee
for Aeronautics.

TABLE II. Wooden Spar II. Influence values δ_{ik} (deflections) for making the calculation plotted in Figure 26. Determined from static tests

150 kg (330 lb.) on rib \ Deflections at rib (mm × 10^{-1})	2	3	4	5	6	7	8	9	10	11
2	7	11	14.5	17	18	17	16	13.5	11	9
3	11	19	25.5	30	31.5	31	29	25.5	21.5	17
4	14.5	25.5	34.5	41.5	44	43.5	40.5	36.5	30.5	24.5
5	17	30	41.5	50	54	54	50.5	45	38	30
6	18	31.5	44	54	58.5	60	58	52	44.5	35
7	17	31	43.5	54	60	63	62	57	48	38
8	16	29	40.5	50.5	58	62	62.5	58	49	39
9	13.5	25.5	36.5	45	52	57	58	54.5	47	37.5
10	11	21.5	30.5	38	44.5	48	49	47	44	35.5
11	9	17	24.5	30	35	38	39	37.5	35.5	30
12	6	12	17	21	24	26.5	27	26.5	25.5	21
13	3	6	9	11	13	14.5	14.5	14	13.5	11
14	0	0	0	0	0	0	0	0	0	0
15	- 3	- 6	- 8.5	-11	-13	- 13.5	-15	-14.5	- 13.5	-11.5
16	- 7	-12	-18	-22	-26	- 27	-28.5	-28	- 26	-22
17	-10	-18.5	-27	-32	-37.5	- 40	-42	-41	- 39	-34
18	-13	-25	-36	-43.5	-50.5	- 53.5	-57	-55.5	- 52.5	-44
19	-17	-32	-46	-54.5	-63.5	- 68	-73	-68	- 67	-53
20	-20.5	-39	-55.5	-66	-77	- 82	-88	-82.5	- 80.5	-61
21	-24.5	-45.5	-65	-77	-88.5	- 95	-102.5	-96	- 93	-78

TABLE II. (Cont'd) Wooden Spar II. Influence values δ_{ik} (deflections) for making the calculation plotted in Figure 26. Determined from static tests

Deflections at rib ($mm \times 10^{-1}$) / 150 kg (330 lb.) on rib	12	13	14	15	16	17	18	19	20	21
2	6	3	0	- 3	- 7	-10	-13	17	20.5	24.5
3	12	6	0	- 6	-12	-18.5	-25	32	39	45.5
4	17	9	0	- 8.5	-18	-27	-36	46	55.5	65
5	21	11	0	-11	-22	-32	-43.5	54.5	66	77
6	24	13	0	-13	-26	-37.5	-50.5	63.5	77	88.5
7	26.5	14.5	0	-13.5	-27	-40	-53.5	68	82	95
8	27	14.5	0	-15	-28.5	-42	-87	73	88	102.5
9	26.5	14	0	-14.5	-28	-41	-55.5	68	82.5	96
10	25.5	13.5	0	-13.5	-26	-39	-52.5	67	80.5	93
11	21	11	0	-11.5	-22	-34	-44	55.5	67.5	78
12	16.5	8.5	0	- 9	-17	-24.5	-33	44	53	61
13	8.5	4.5	0	- 5	- 9	-13	-18	22.5	27.5	31.5
14	0	0	0	0	0	0	0	0	0	0
15	- 9	- 5	0	5	11	16	19	24	29.5	34
16	-17	- 9	0	11	22.5	35.5	48	61	74	85.5
17	-24.5	-13	0	16	35.5	57	80	102	125	145
18	-33	-18	0	19	48	80	112	145.5	179	211
19	-44	-22.5	0	24	61	102	145.5	190	231.5	275.5
20	-53	-27.5	0	29.5	74	125	179	231.5	290	345.5
21	-61	-31.5	0	34	85.5	145	211	275.5	345.5	408

TABLE III. Steel Spar I. Results of endurance tests with whole spar. Load reversals and stresses in the most unfavorable cross section and in the breaking cross section

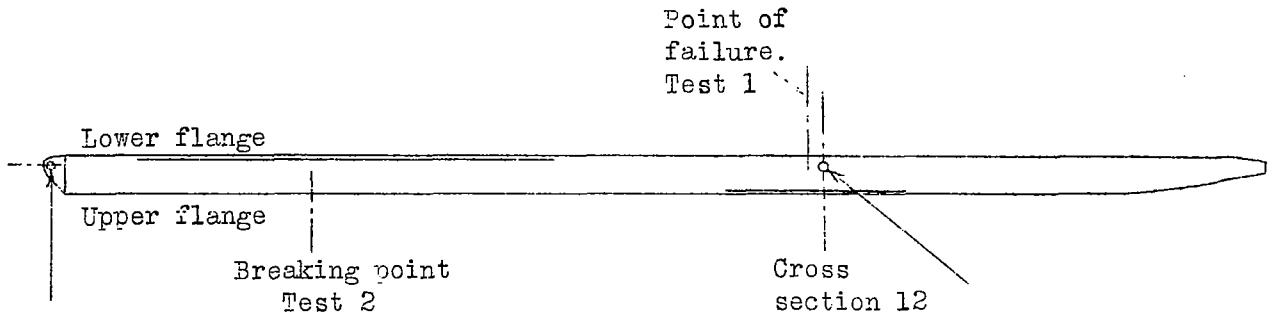

Time	Frequency	Number of reversals n	Max. amplitude a	Flange	Flange stresses in max. stressed section 12				Flange stresses at point of failure			
					static	dynamic	superposed		static	dynamic	superposed	
Min	1/min		cm		kg/mm²	kg/mm²	kg/mm²		kg/mm²	kg/mm²	kg/mm²	
180	980	177,000	3.2	upper	- 8.5	∓ 4.0	-12.5	- 4.5	-9.0	∓ 4.1	-13.1	-4.9
				lower	+14.4	± 6.6	+21.0	+ 7.8	+8.5	± 6.1	+14.6	+2.4
450	980	441,000 (until failure)	4.44 to 5.9	upper	- 8.5	∓ 5.5	-14.0	- 3.0	-9.0	∓ 5.7	-14.7	-3.3
				lower	+14.4	+ 9.2	+23.6	+ 5.2	+8.5	± 8.5	+17.0	0
				upper	- 8.5	∓ 7.3	-15.8	- 1.2	-9.0	∓ 7.6	-16.6	+1.4
				lower	+14.4	±12.2	+26.6	+ 2.2	+8.5	±11.3	+19.8	-3.8
									Breaking stresses			

Total reversals n = 618,000

TABLE IV. Steel Spar I. Inner bay without overhang. Load reversals and stresses in the most unfavorable cross section and in the breaking cross section

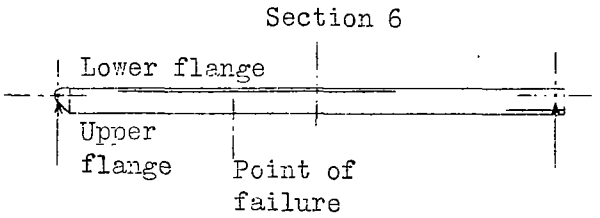

Time	Frequency ω	Number of reversals n	Max. amplitude a	Flange	Flange stresses							
					in max. stressed section 12			at point of failure				
					static	dynamic	superposed	static	dynamic	superposed		
					kg/mm²	kg/mm²	kg/mm²	kg/mm²	kg/mm²	kg/mm²		
Min	l/min		cm									
180*	980	177,000	-	upper	+ 5.3	∓ 6.5	- 1.2	+11.8	+6.0	∓ 5.0	+ 1.0	+11.0
				lower	- 7.0	± 3.4	- 3.6	-10.4	-7.0	± 2.5	- 4.5	- 9.5
450*	980	441,000		upper	+ 5.3	∓ 9.0	- 3.7	+14.3	+6.0	∓ 7.0	- 1.0	+13.0
				lower	- 7.0	± 4.7	- 2.3	-11.7	-7.0	± 3.5	- 3.5	-10.5
				upper	+ 5.3	∓12.0	- 6.7	+17.3	+6.0	∓ 9.3	- 3.3	+15.3
				lower	- 7.0	± 6.2	- 0.8	-13.2	-7.0	± 4.6	- 2.4	-11.6
95	1,400	133,000	1.5	upper	0	± 6.8	+ 6.8	- 6.8	0	± 6.2	+ 6.2	- 6.1
				lower	0	∓ 4.1	- 4.1	+ 4.1	0	∓ 3.7	- 3.7	+ 3.7
37	1,400	51,800	1.6	upper	+10.0	± 7.3	+17.3	+ 2.7	+9.3	± 6.6	+15.9	+ 2.7
				lower	- 6.0	∓ 4.3	-10.3	- 1.7	-5.5	∓ 3.9	- 9.4	- 1.6
60	1,400	84,000	2.0	upper	+10.0	± 9.1	+19.1	+ 0.9	+9.3	± 8.2	+17.5	- 1.1
				lower	- 6.0	∓ 5.4	-11.4	- 0.6	-5.5	∓ 4.9	-10.4	- 0.6
35	1,400	49,000 (until failure)	2.1 to 2.35	upper	+10.0	± 9.6	+19.6	+ 0.4	+9.4	± 8.7	+18.1	+ 0.7
				lower	- 6.0	∓ 5.7	-11.7	- 0.3	-5.5	∓ 5.2	-10.7	- 0.3
				upper	+10.0	±10.7	+20.7	- 0.3	+9.3	± 9.7	+19.0	- 0.4
				lower	- 6.0	∓ 6.4	-12.4	+ 0.4	-5.5	± 5.8	-11.3	+ 0.3

Total reversals n = 935,800

*Load reversals and stresses suffered by middle section of spar in first test.

TABLE V. Steel Spar II. Whole spar and overhang.
Load reversals and stresses in breaking cross section.

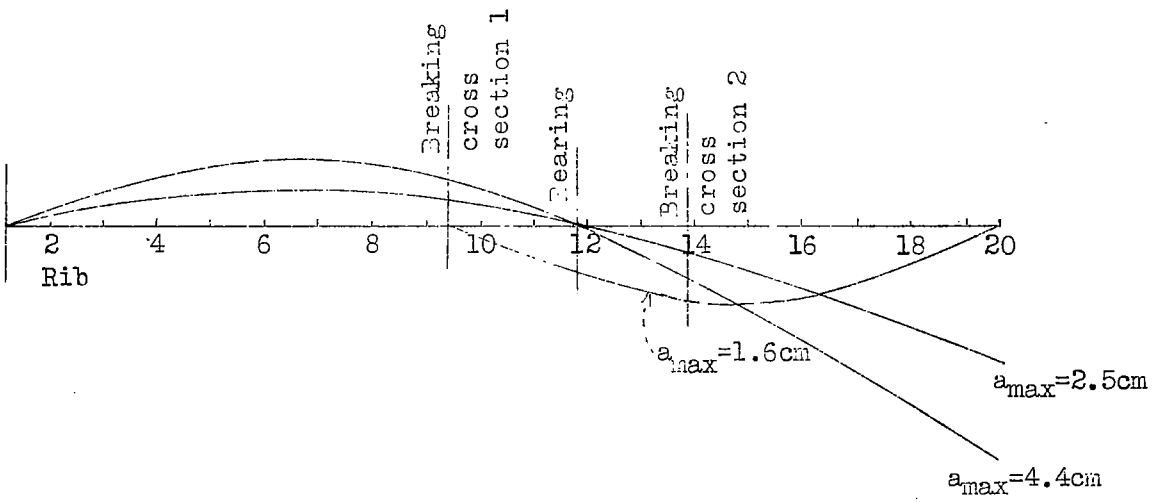

Test	Frequency 1/min	Number of reversals n 10^6	Max. amplitude a cm	Flange	Breaking cross section 1				Breaking cross section 2			
					static kg/mm²	dynamic kg/mm²	superposed kg/mm²		static kg/mm²	dynamic kg/mm²	superposed kg/mm²	
Whole spar	940	2.15	2.5	upper	-8.6	∓9.0	-17.6	+0.4	-11.4	∓5.2	-16.6	-6.2
				lower	+1.6	±8.1	+ 9.6	-6.5	+11.4	±5.2	-16.6	+6.2
	925	0.70	4.4	upper	-8.6	∓15.4	-24.0	+6.8	-11.4	∓8.9	-20.3	-2.5
				lower	+1.6	±13.9	+15.5	-12.3	+11.4	±8.9	+20.3	+2.5
Piece of spar	1,600	0.058	1.6	upper	-	-	-	-	-	∓16.0	-	-
				lower	-	-	-	-	-	±16.0	-	-

TABLE VI. Steel Lattice Spars
Load reversals and breaking stresses.
Location of breaking point. (Fig. 39.)

Spar number	Load reversals 10^6	Stresses in breaking section			Breaking point	
		static kg/mm^2	dynamic kg/mm^2	superposed kg/mm^2	Location	Picture
1	2.29	-0.1	± 4.6	+4.5 -4.7	plate	a
2a	2.63 0.314	- -	± 2.4 ± 3.1	- -	joint	b
2b	2.9 2.23 1.88	- - -	break 1 ± 1.7 ± 2.1 ± 3.0	break 2 ± 1.8 ± 2.3 ± 3.2	2) plate 1) in bulge	like a c
3	0.46	-	± 2.4	-	plate	like a

Breaks 1 and 2 occurred simultaneously in spar 2b.

TABLE VII. Wooden Spar I (Spruce). Load reversals and stresses in breaking cross section

Time T min	Frequency 1/min	Number of reversals n	Max. amplitude a cm	Flange	Flange stresses in breaking cross section: static kg/cm^2	dynamic kg/cm^2	superposed kg/cm^2		Temperature °C	Relative humidity of air per cent
Preliminary test 96	1,020-1,130	about 1.03×10^5	1.85	upper lower	- -	- -	- -	- -	-	-
1,005	1,120	11.25×10^5	3.85	upper lower	-15 +15	$\mp$ 75 $\pm$ 75	- 90 + 90	+ 60 - 60	4 to 9.4	62 to 76
565	1,060	6.00×10^5	6.40	upper lower	-15 +15	$\mp$125 $\pm$125	-140 +140	+110 -110	7 to 12.8	62
130	1,035	1.35×10^5	11.40	upper lower	-15 +15	$\mp$225 $\pm$225	-240 +240	+210 -210	11	63

Total reversals: $n = 19.63 \times 10^5$

TABLE VIII. Wooden Spar II (Pine) Load reversals and stresses in breaking cross section

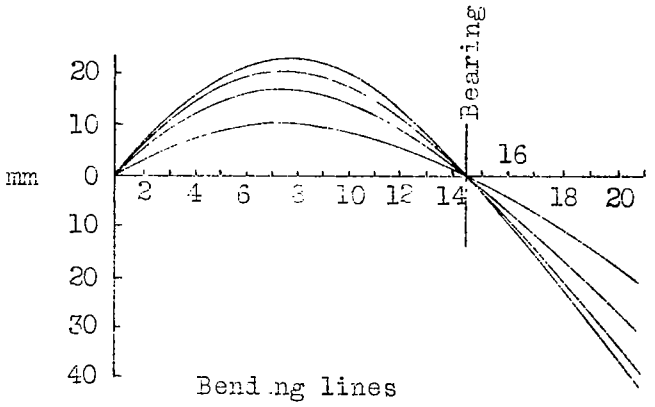

Test	Load n_A	Max. amplitude a_{max} mm	Frequency ω 1/min	Number of reversals n 10^6	Flange	Max. stresses at rib 6 static kg/cm²	at rib 6 dynamic kg/cm²	at rib 8 static kg/cm²	at rib 8 dynamic kg/cm²	at rib 15 static kg/cm²	at rib 15 dynamic kg/cm²	Remarks
2	1.3	44	1,075	3.0	upper	+ 72	∓109	+ 44	∓ 96	- 55	∓ 24	no break
					lower	- 63	± 54	- 59	± 66	+ 75	± 33	
3	2.0	66	1,075	2,024	upper	+110	∓163	+ 67	∓144	- 85	∓ 36	no break
					lower	- 96	± 81	- 90	± 99	+115	± 49	
4a	2.6	80	1,075	1,946	upper	+143	∓198	+ 87	∓175	-110	∓ 44	no break
					lower	-125	± 99	-117	±120	+149	± 59	
4b	2.6	90	1,035	2,534	upper	+143	∓207	+ 87	∓182	-110	∓ 46	(Break 1 near unbalance shortly after beginning of test. Break 2 occurred immediately after repairing.)
					lower	-125	±103	-117	±125	+149	± 68	
4c	2.6	110	1,020	-	upper	+143	∓245	+ 87	∓216	-110	∓ 54	(Broke at beginning near unbalance.)
					lower	-125	±122	-117	±148	+149	± 73	

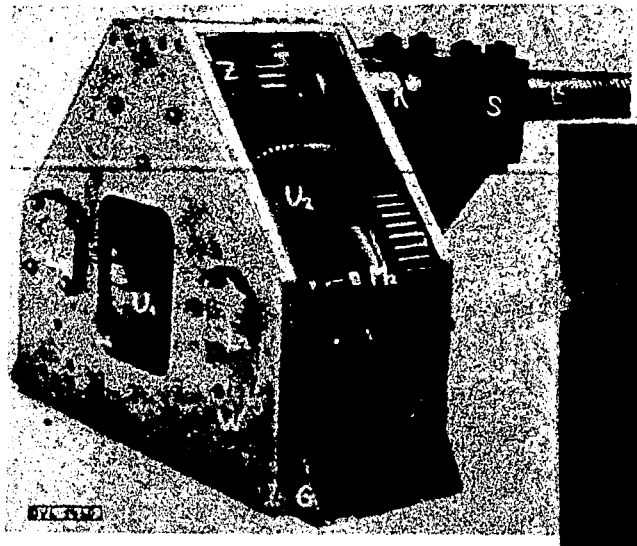

Figure 1.-Double unbalance.

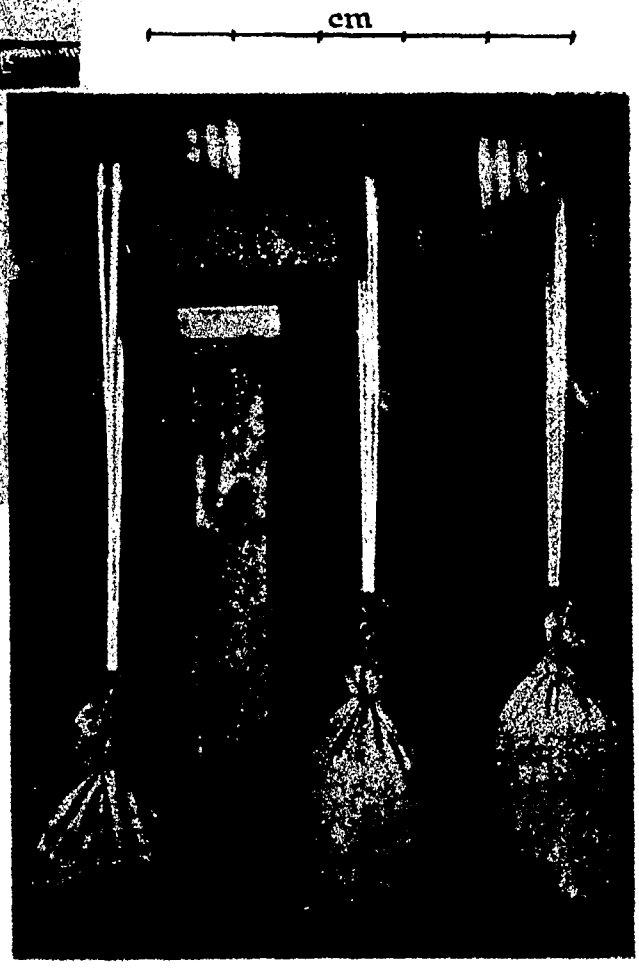

Figure 2.-Vibrating spar tip with superposed static load. Spar I. Exposure, 1 sec. The amplitude is read on the test wedges, outwardly 5.4 cm(2.13 in.) Superposed static load at rest.

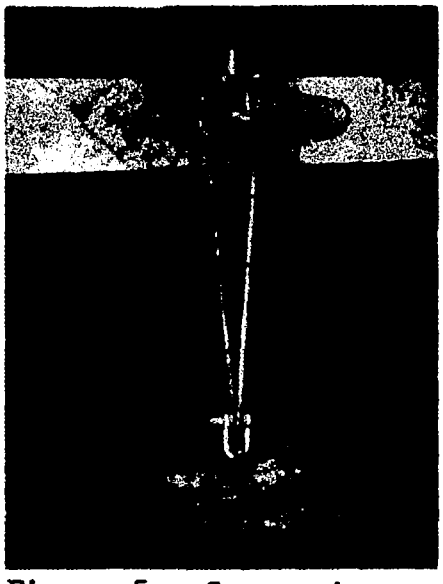

Figure 5a.-Suspension device for superposed static load.

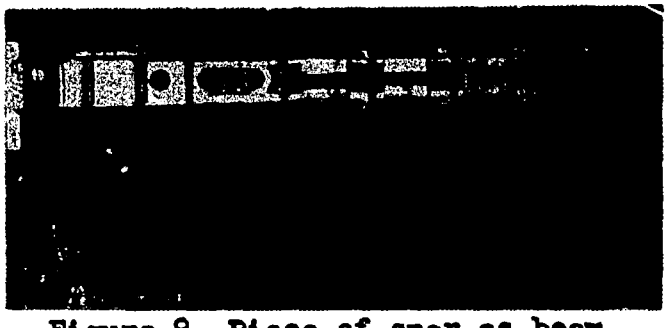

Figure 9.-Piece of spar as beam on two supports.

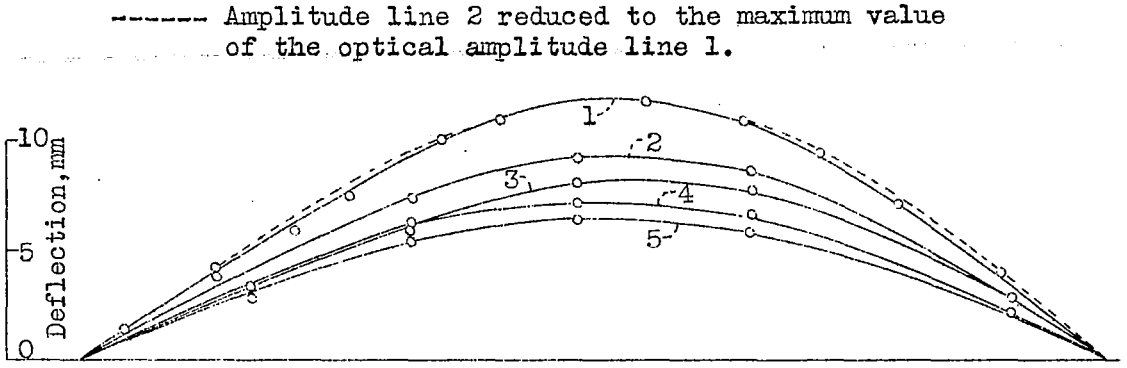

Figure 3.-Comparison of bending lines in vibration, as measured by test wedges and optographs. Steel spar I. Inner field.
1, Obtained with test wedges.
2,3 With optographs before beginning of break.
4,5 " " after " " " .

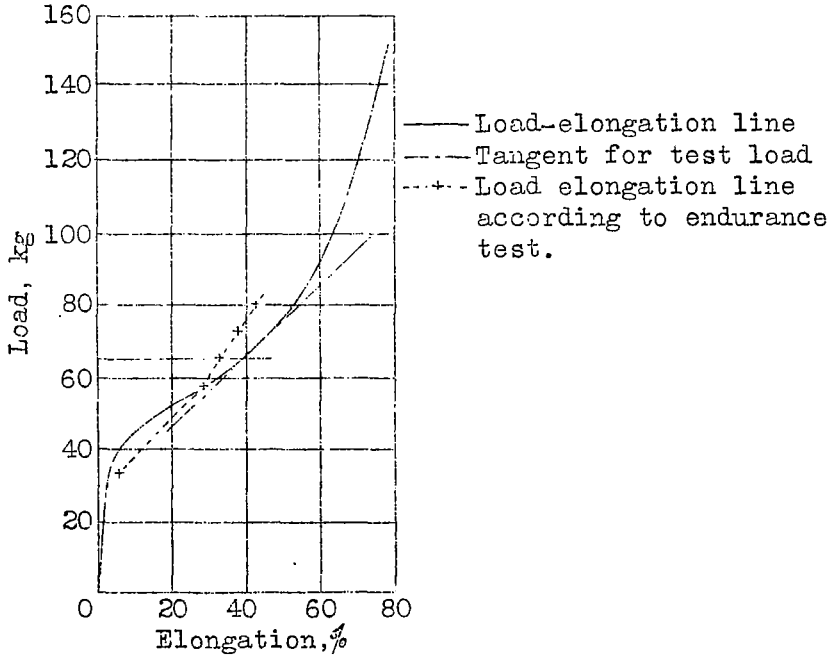

Figure 4.-Load-elongation line of the rubber cord used for the superposed static load. Diameter 17 mm (0.67 in.) Number of strands 800.

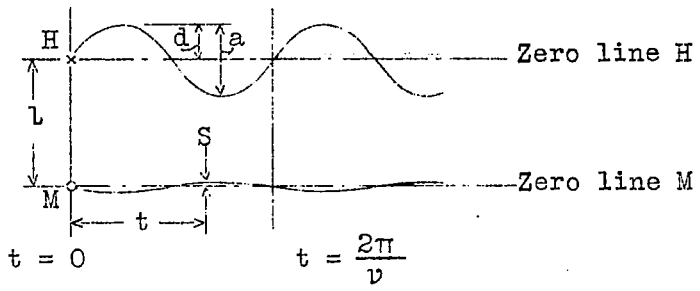

Figure 5b.-Diagram of the vibration phenomenon.

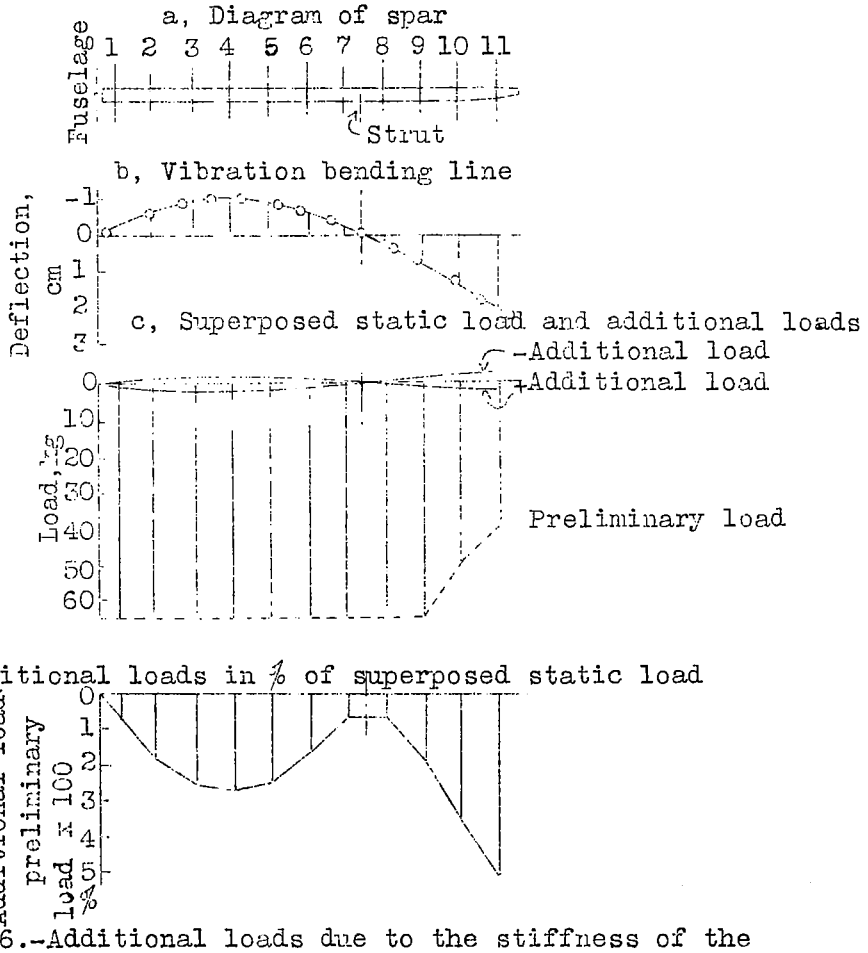

Figure 6.-Additional loads due to the stiffness of the rubber cord. Wooden spar II.

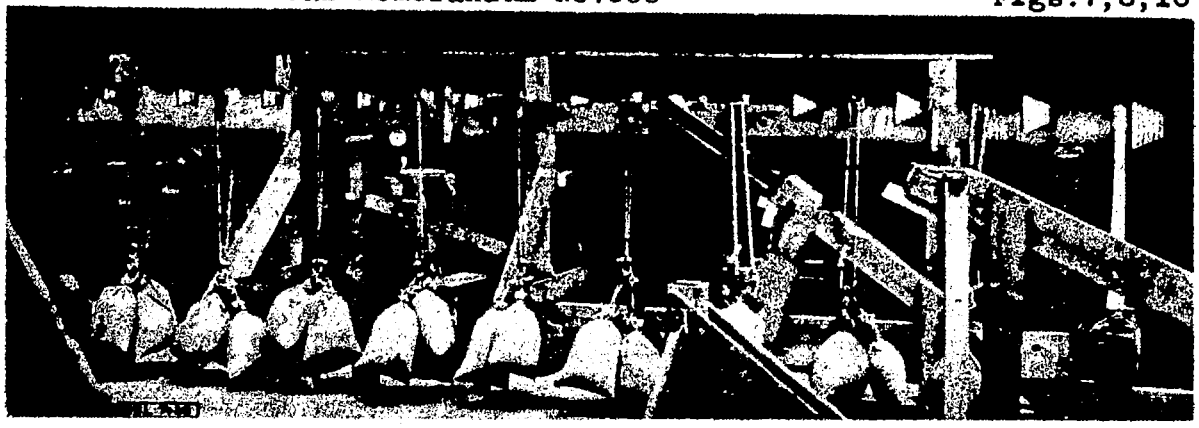

Figure 7.-Vibration test with superposed static load. Wooden spar II (vibrating). Double unbalance at the left and behind it the direct-current motor with tachometer.

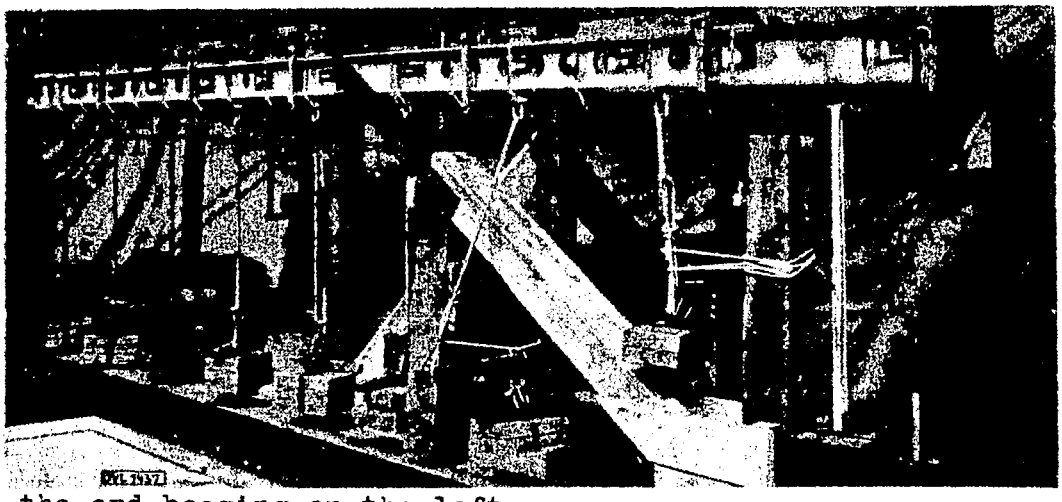

Fig.8 - Vibration test with superposed static load. Elektron spar (vibrating). Single unbalance at the end bearing on the left.

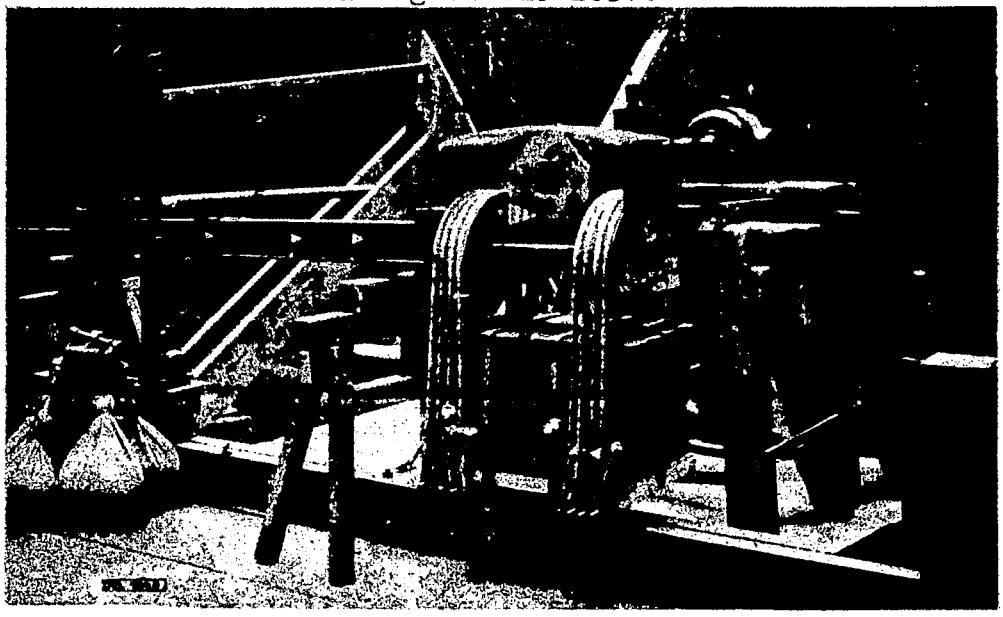

Figure 10- Endurance-test apparatus for structural parts (16000 kg= 35,274 lb. apparatus)

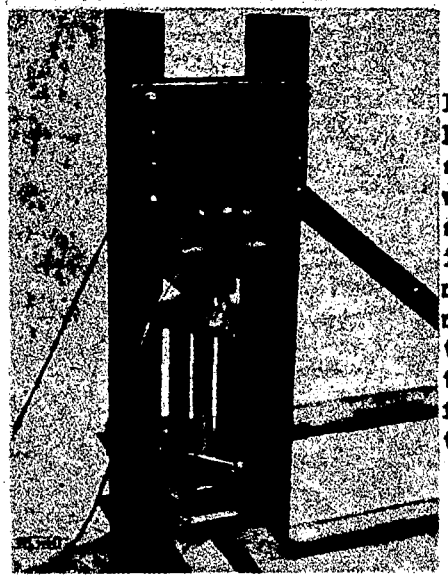

Figure 11 Pendulum support with two scratch instruments for measuring the vibration forces in the support

Figure 12.-Former endurance-test apparatus. Two structural parts are being tested simultaneously. A spar fitting is mounted at the support A. (See Fig.13) A connecting rod is mounted at B.

Figure 13.-A connecting rod is mounted at B.

Figure 14. Vibration device in operation. Apparatus for testing a spherical head bolt. Arrangement with superposed static load(original strength)

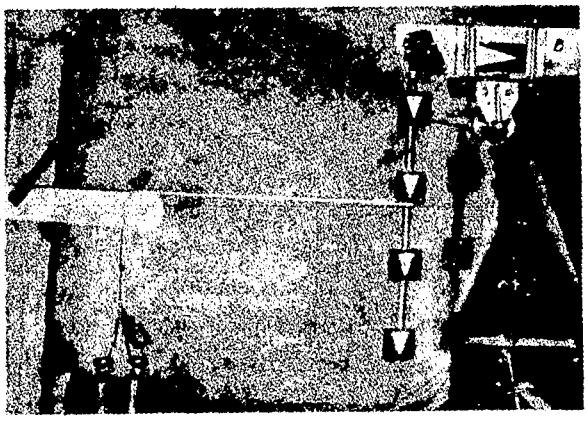

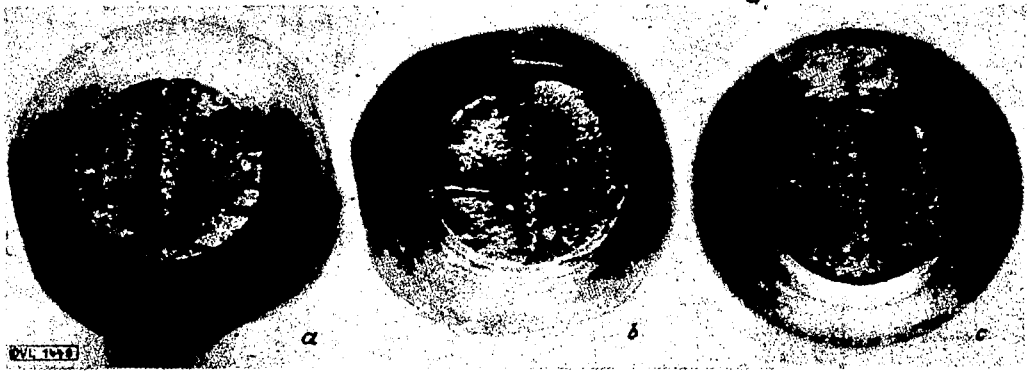

Figure 15.-Test results with the vibration apparatus. Breaks of bolts with spherical heads. a, Break on an airplane in flight. b, Break from simple alternating loading in laboratory. c, Break produced in vibration test of original strength in laboratory.

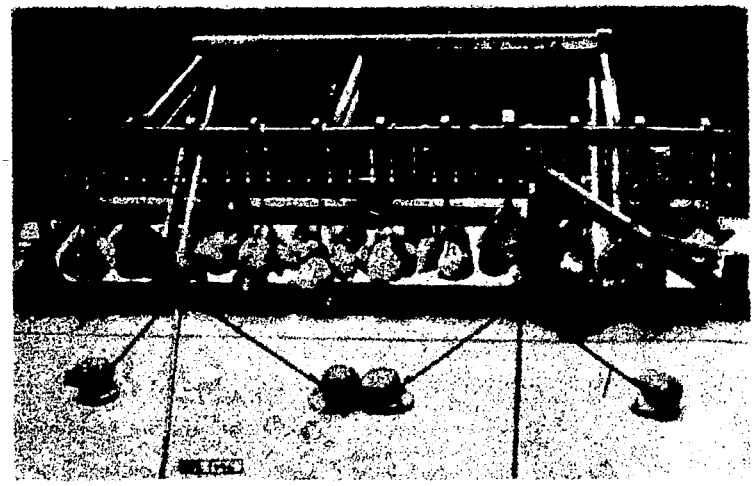

Figure 16-Steel spar I. Static-test installation. Leveling instruments, measuring strips, tensometers.

Figure 19.-Steel spar I. Scratch-instrument record. Magnification about 150 fold.

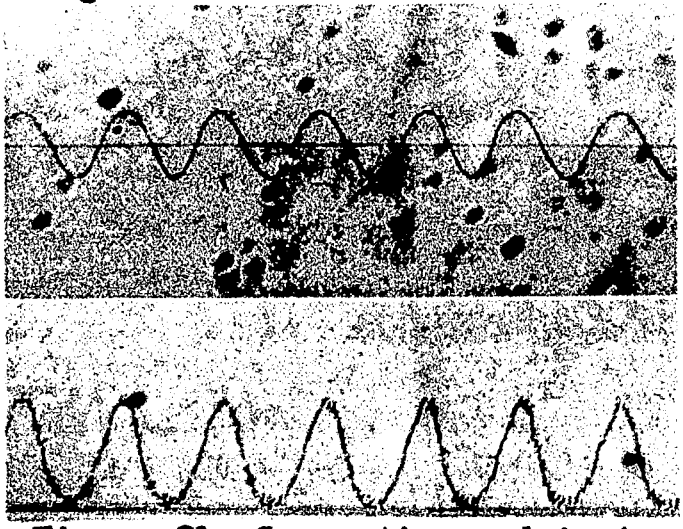

Figure 21.-Connecting-rod test. Scratch record. Magnification about 130 fold. 1 mm = a force of 680 kg in connecting rod.

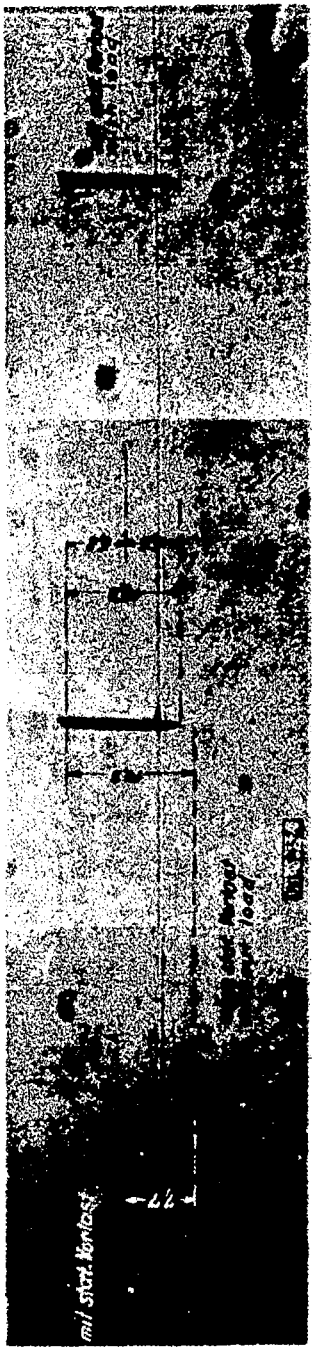

Figure 22.-Connecting-rod test. Scratch records. Magnification about 120 fold. Elongation in test bar due to preliminary static loading and superposed vibrations.

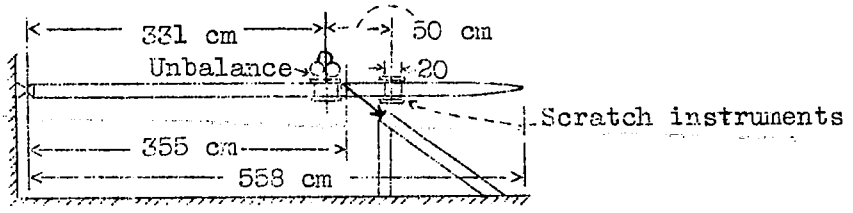

Figure 17.- Steel spar I. Installation for vibration test with scratch- instrument measurements.

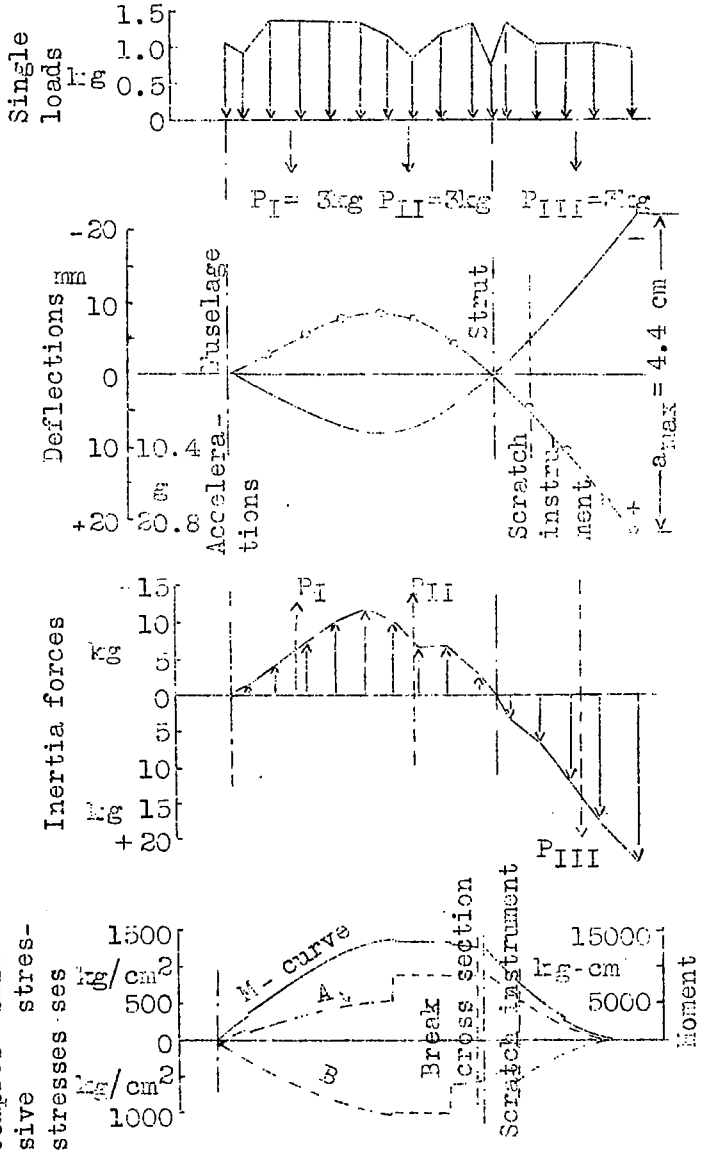

(a) Spar weights, parallel guides P_I to P_{III}

(b) Vibration bending line (= accelaea- tion line)

(c) Inertia forces for + bending line with $a_{max.}$ = 4.4 cm(1.73 in.)

A, Lower-flange stresses
B, Upper-flange stresses

(d) Moments and flange stresses from dynamic load for + bending line with $a_{max.}$ = 4.4cm(1.73 in.)

Figure 18.- Steel spar I. Test results. Determination of accelerations and dynamic stresses. n =980/min. $a_{max.}$ = 4.4 cm(1.73in.)

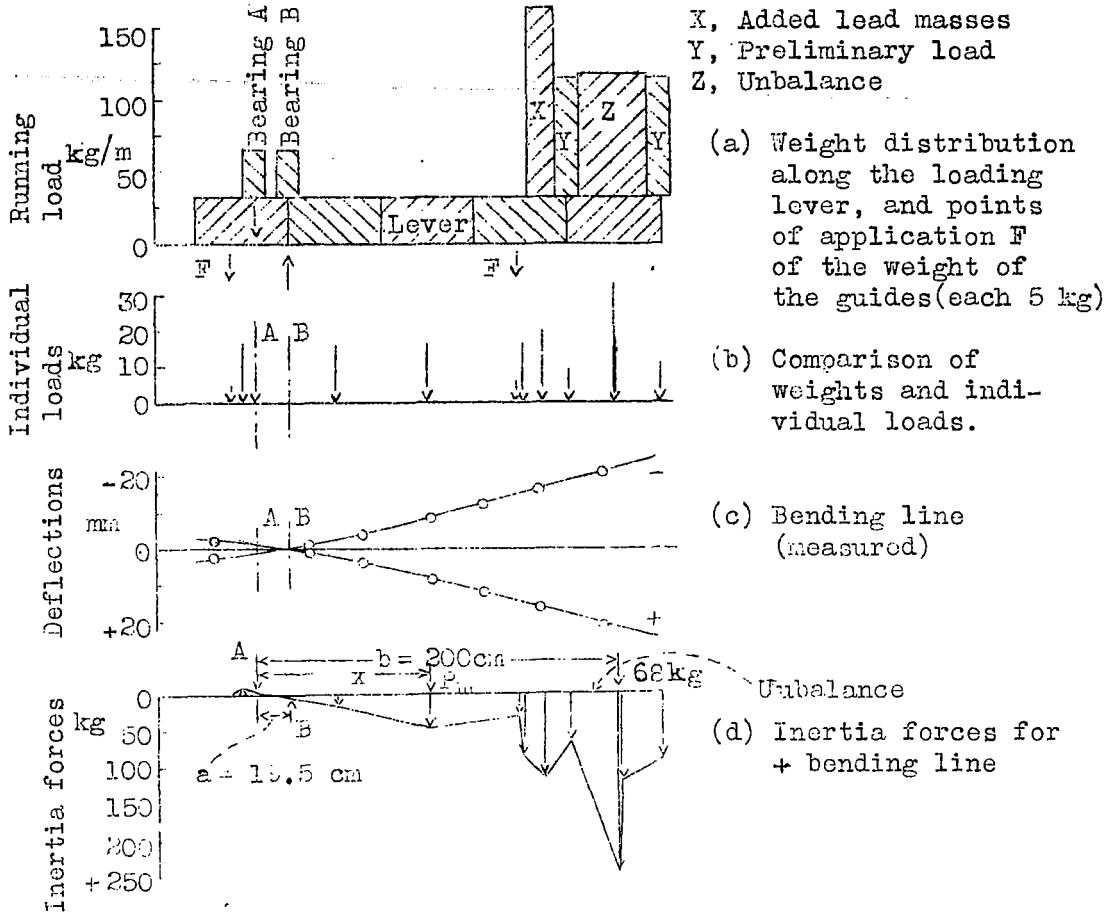

Figure 20.- Endurance test of a connecting rod. Determination of the inertia forces from the bending line of the lever. ω = 560/min.

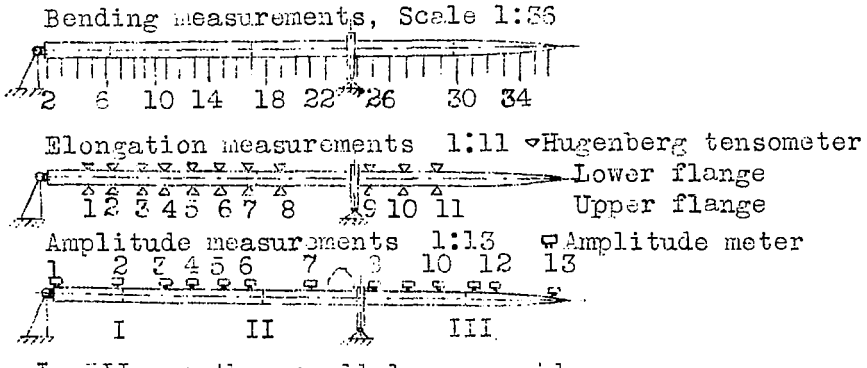

I - III are the parallel spar guides.

Figure 23.- Wooden spar I. Arrangement for static and dynamic tests.

(a) Load distribution, preliminary static test.

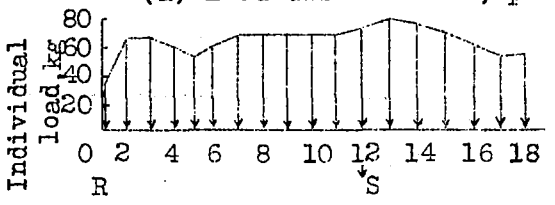

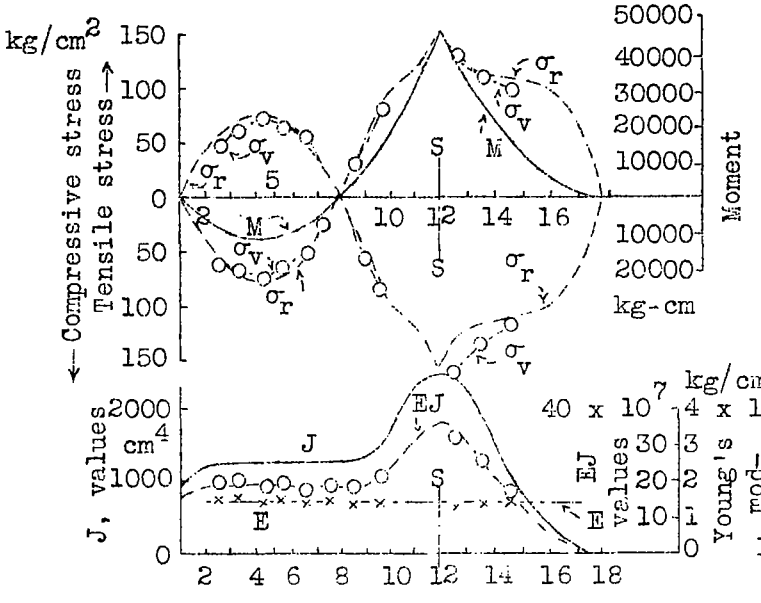

(b) Comparison of calculated and measured M_1 moments. Flange stresses σ.

---- σ_r calculated

—— σ_v measured

(c) J and EJ values, Young's modulus

Fig. 24 Wooden spar I. Vibration test. Checking of the inertia-force calculation by calculating the vibration bending line from the inertia forces and the experimental EJ values.

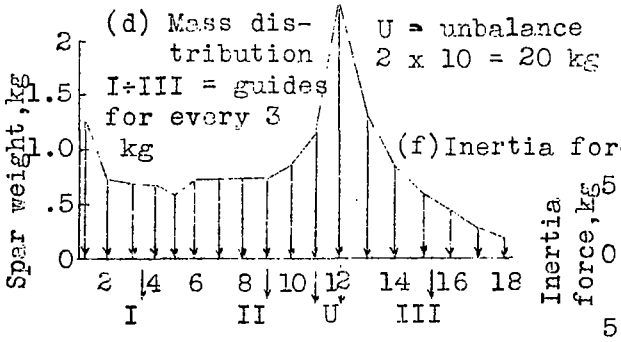

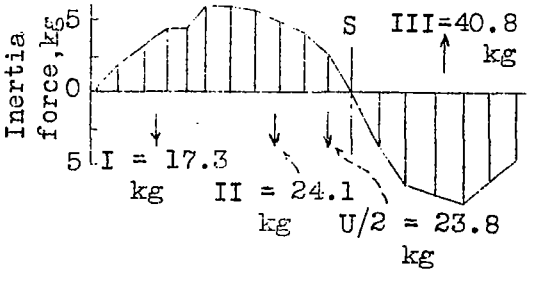

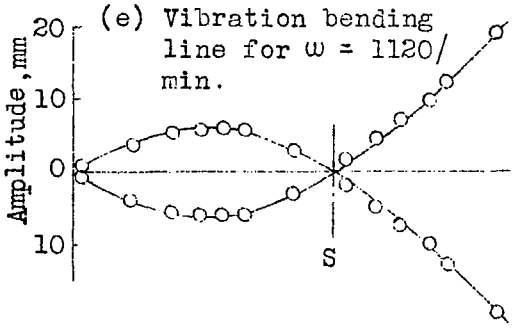

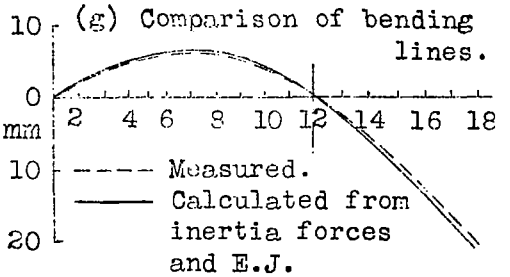

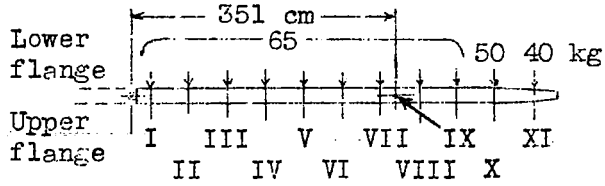

(a) Plan for superposed static load. (n_A = 1.3)

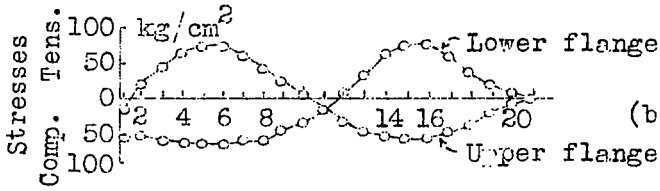

(b) Static flange stresses (n_A = 1.3)

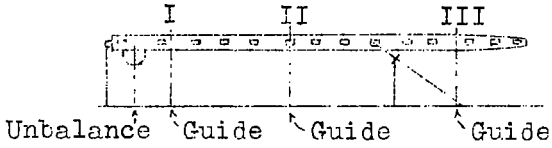

(c) Vibration test plan

▫ Test points.

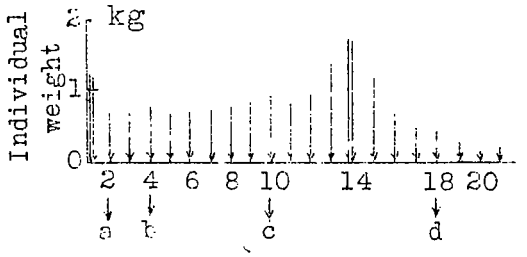

(d) Mass distribution (calculated).

a, U = 29.7 kg
b, I = 2.1 kg
c, II = 2.1 kg
d, III = 2.1 kg

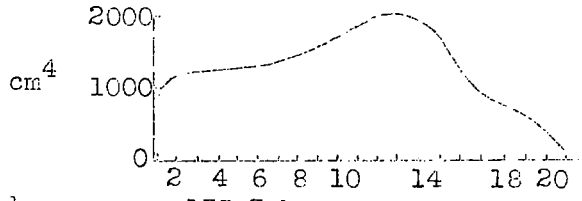

(e) Inertia moments (calculated).

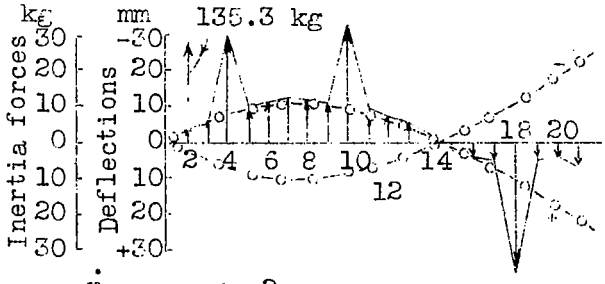

(f) Bending lines and inertia forces (for + bending line).
a_{max} = 4.4 cm

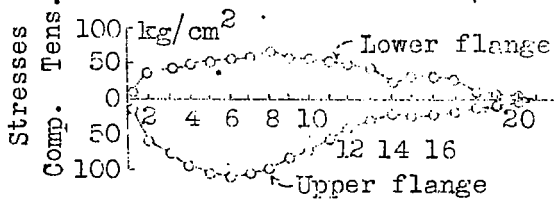

(g) Dynamic flange stresses (for + bending lines).
a_{max} = 4.4 cm

Fig. 25 Wooden spar II. Static and dynamic loading. Determination of stresses.

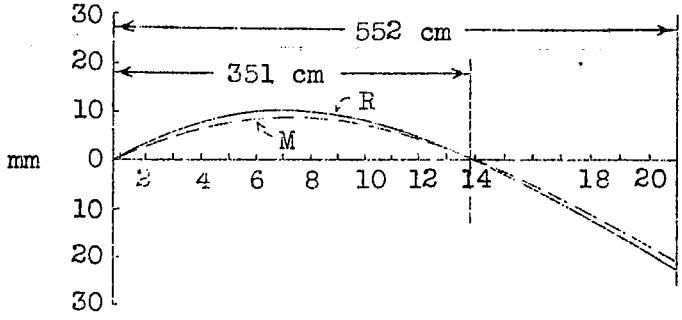

Fig. 26 Wooden spar II. Vibrations bending time. M - measured. R - calculated from inertia forces and influences values (Table II).

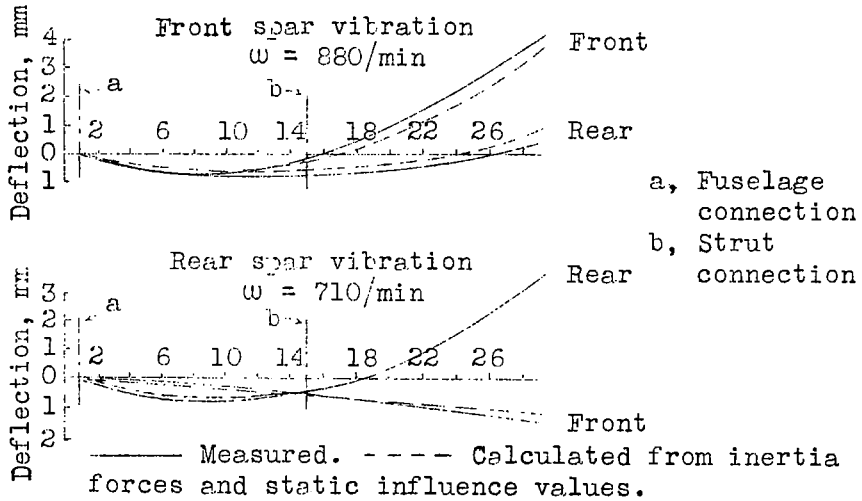

Fig. 27 Wing vibrations. Bending lines in resonance.

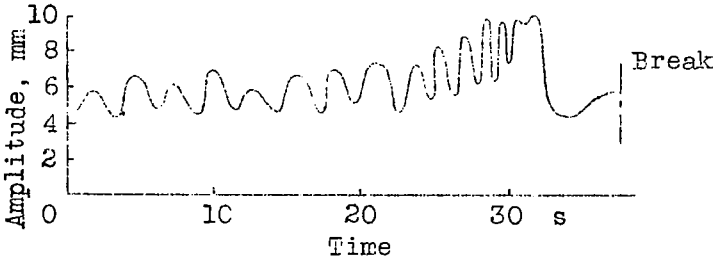

Fig. 29 Steel spar I. Variations in the amplitude after the beginning of the break. Evaluation of an optograph record.

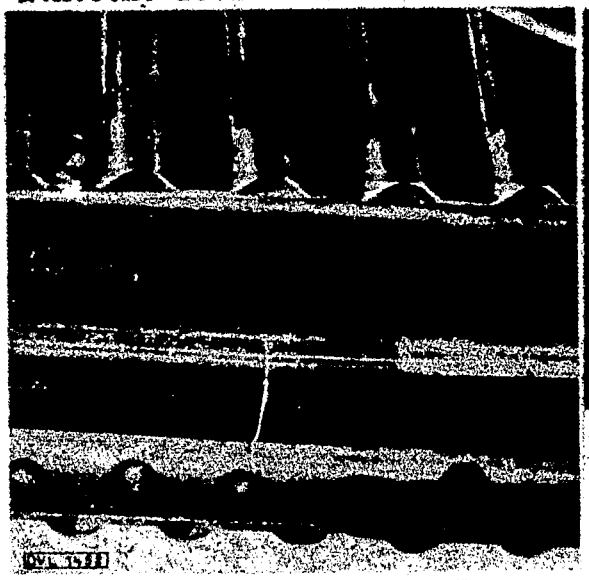

Figure.28-Steel spar I. Dynamic break.

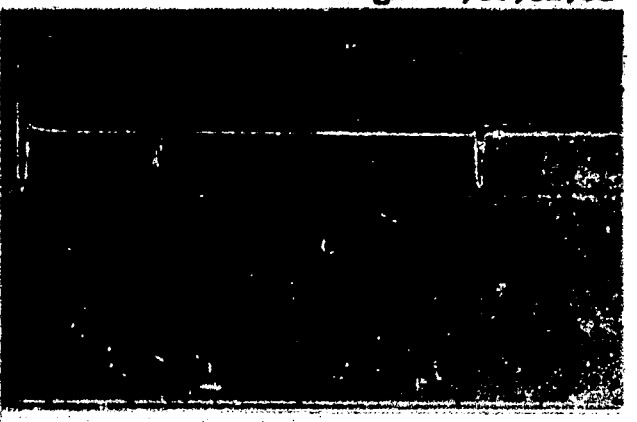

Figure 30.-Steel spar I. Record S of the D.V.L. tachograph shortly before the failure of the spar.(N = zero line.) Scales ordinate, 1cm=290/min., abscissa, 1 cm = 4 min.

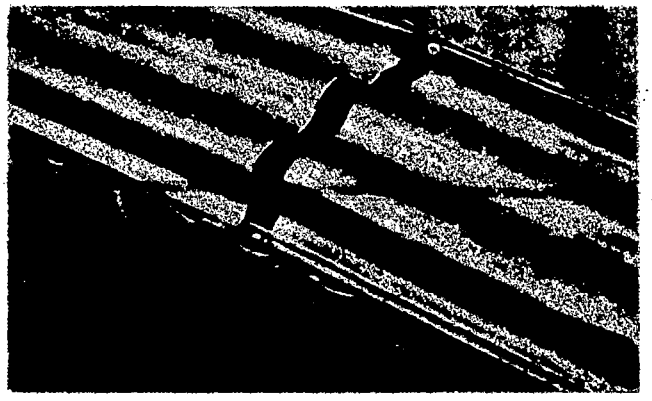

Figure 31 Steel spar I. Fatigue break of flange, beginning at a weld of a strut fitting a.

Figure 33 Steel spar II. Vibration test.

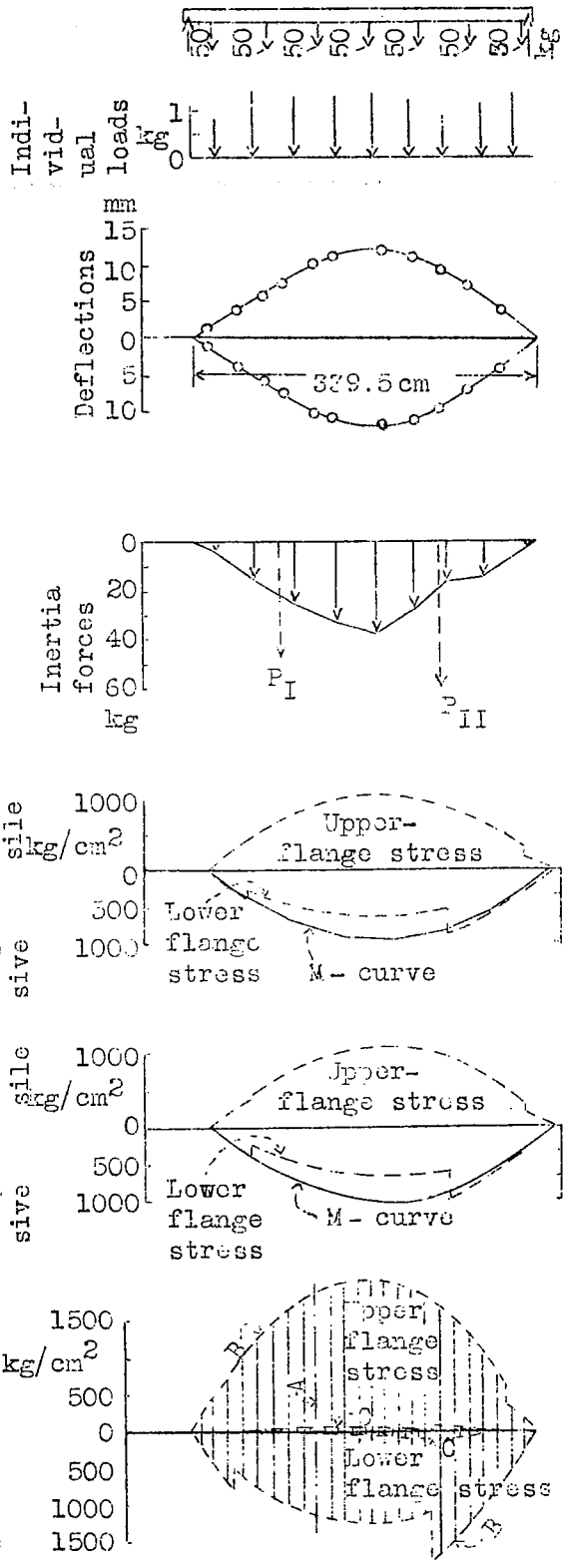

(a) Superposed static load

(b) Mass distribution

(c) Vibration bending line

(d) Inertia forces for + bending line P_I and P_{II} are the inertia forces of the spar guides.

(e) Moments and flange stresses. Superposed static load in the inner bay.

(f) Moments and flange stresses. Superposed static load in the inner bay.

(g) Superposition of static and dynamic stresses.

A, Breaking cross section
B, σ Static+σ dynamic
C, σ static-σ dynamic

Figure 32.- Steel spar I. Inner piece without overhang. Test of original strength with suitable choice of superposed static load. Determination of stresses.

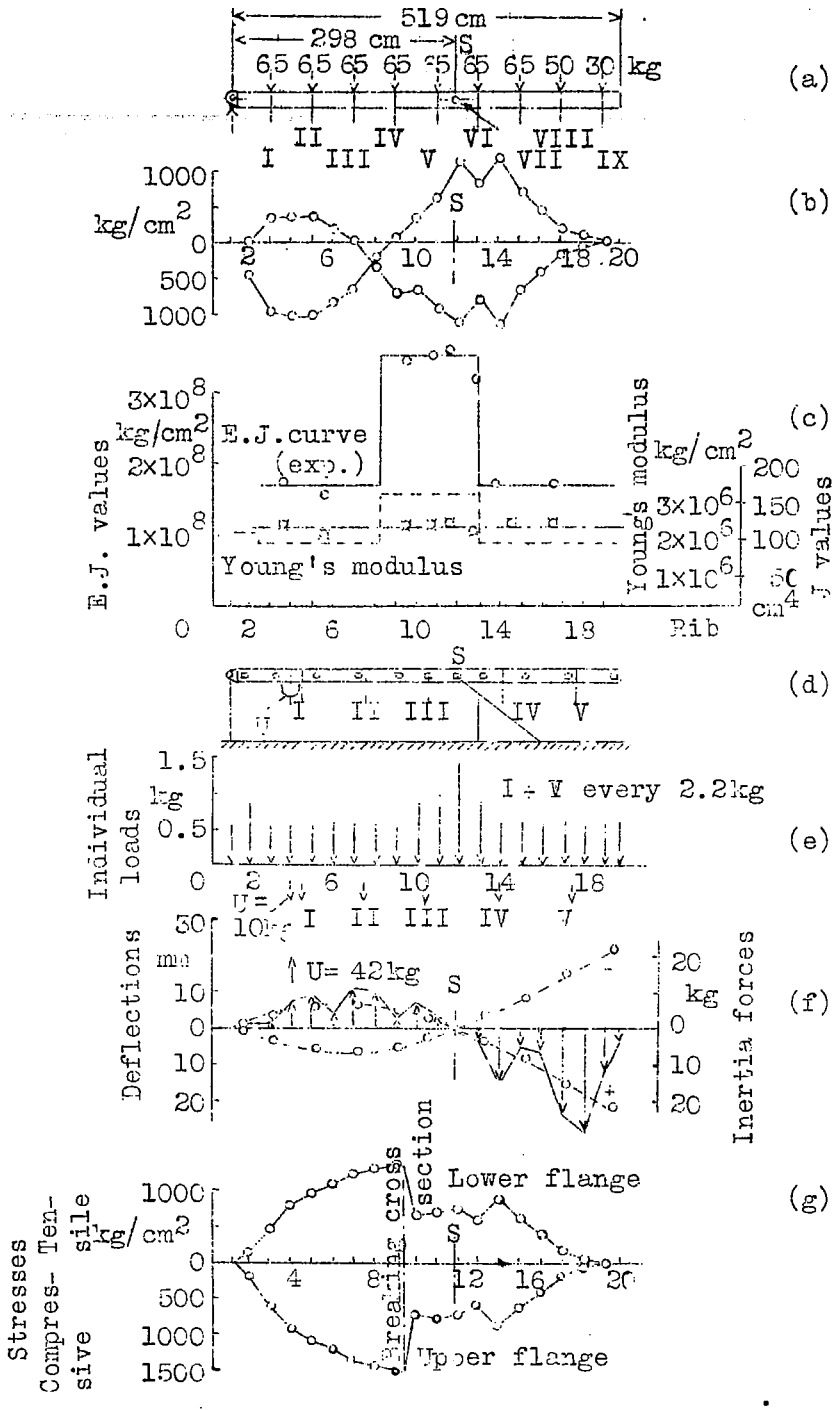

(a) Plan for superposed static load

(b) Static flange stresses

(c) Experimental bending stiffness

(d) Plan for vibration tests

(e) Load distribution

(f) Bending lines and inertia forces

(g) Dynamic flange stresses for $a_{max} = 4.4$ mm, $\omega = 940/\text{min}$.

Figure 34.- Steel spar II. Static and dynamic loading. Determination of bending stiffness and stresses.

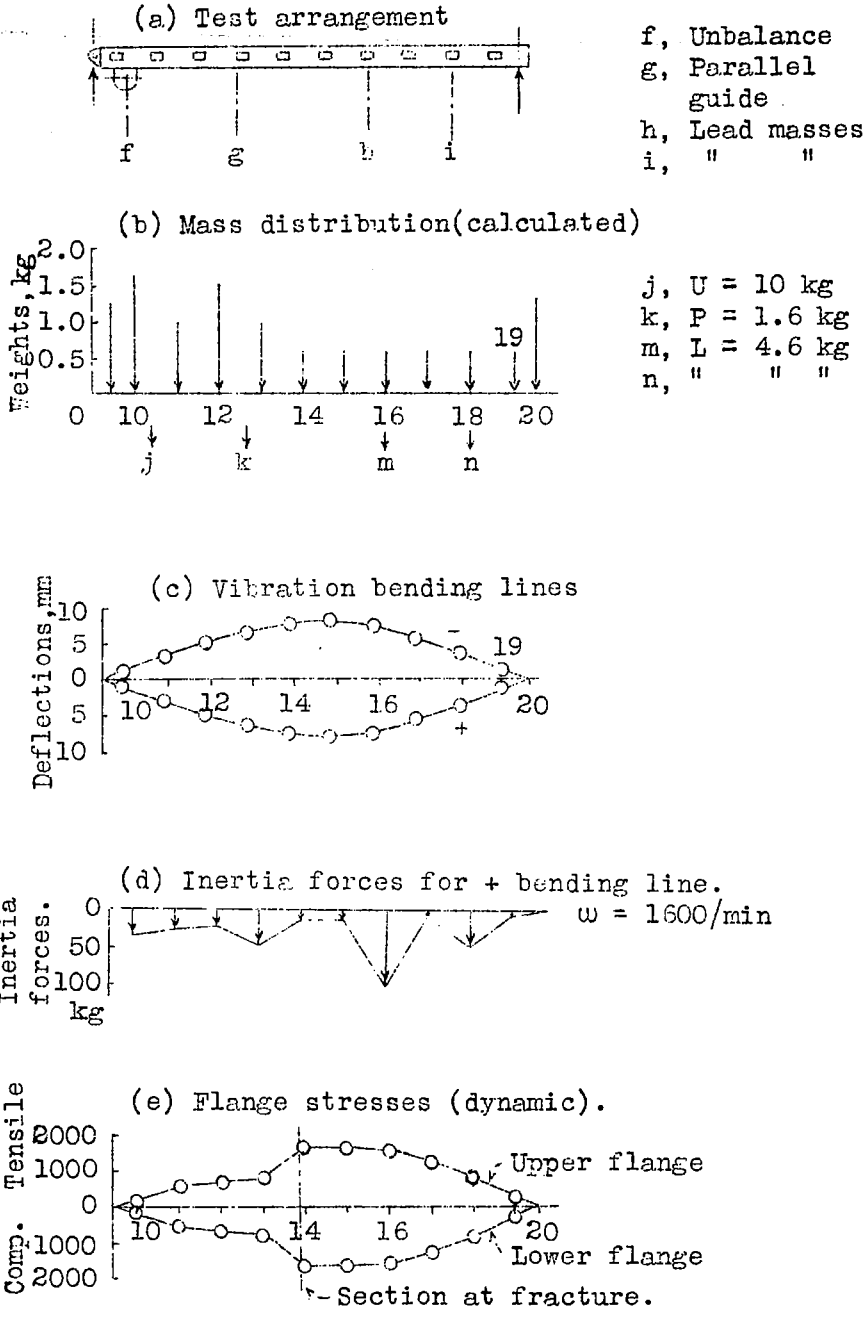

Fig. 35 Steel spar II. Overhang as beam on two supports. Pure dynamic test. Stress determination.

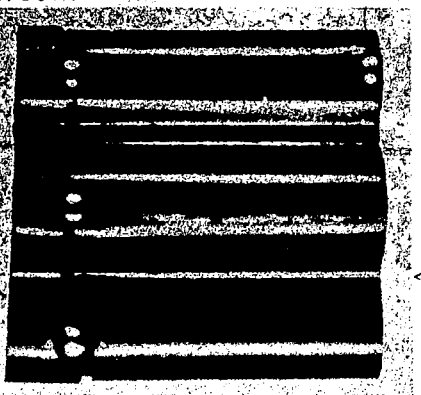

Fig.36
Test I
above,
Test 2
below.

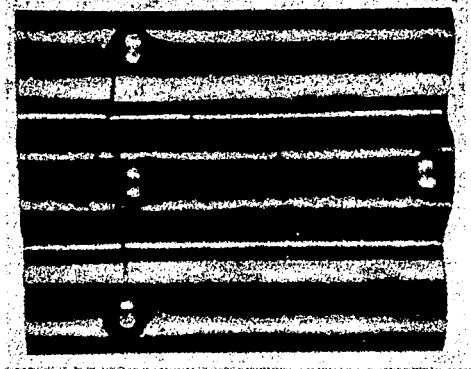

Fig.37
Steel
spar II.

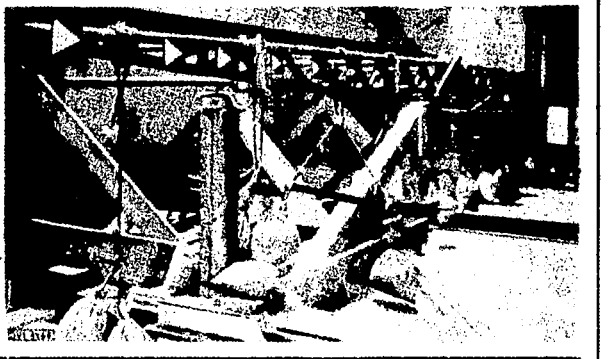

Fig.38

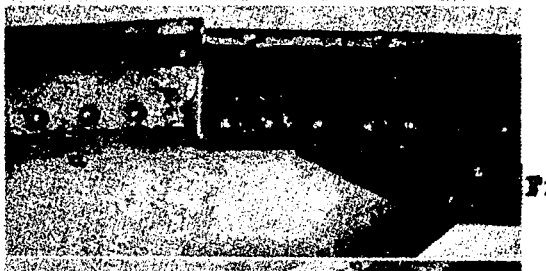

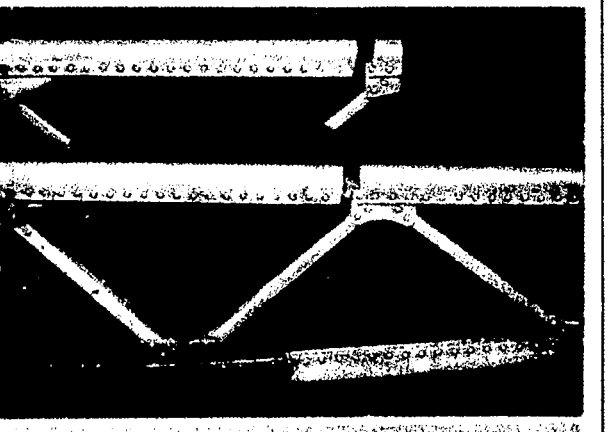

Fig.40

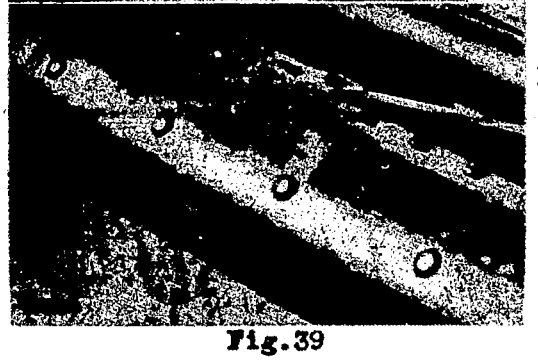

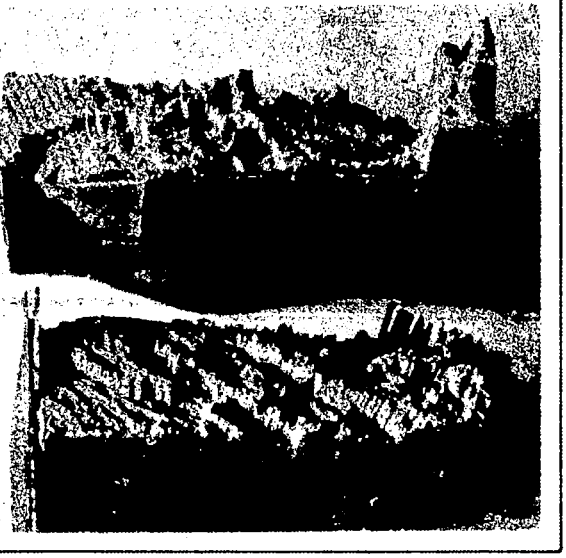

Fig.42
Wooden
spar I

Fig.39

(a) Moments and flange stresses due to the superposed static load.

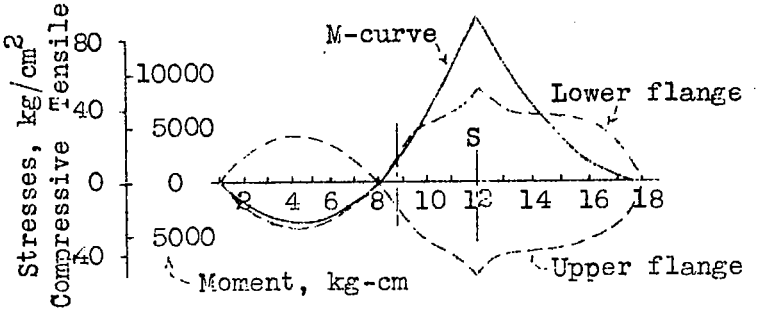

(b) Moments and flange stresses due to spar vibration (+ bending line).

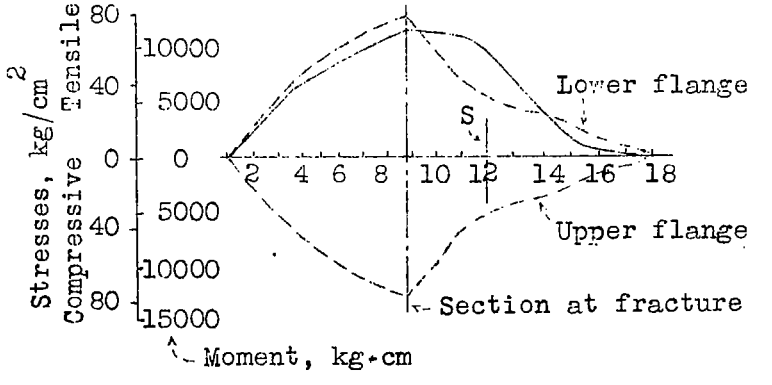

Fig. 41 Wooden spar I. Dynamic stresses and superposed static stresses at ω = 1120/min and a_{max} = 3.85 (Fig. 24).

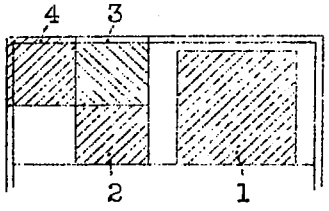

Fig. 43 Wooden spar I. Location of compression cubes cut from flange.

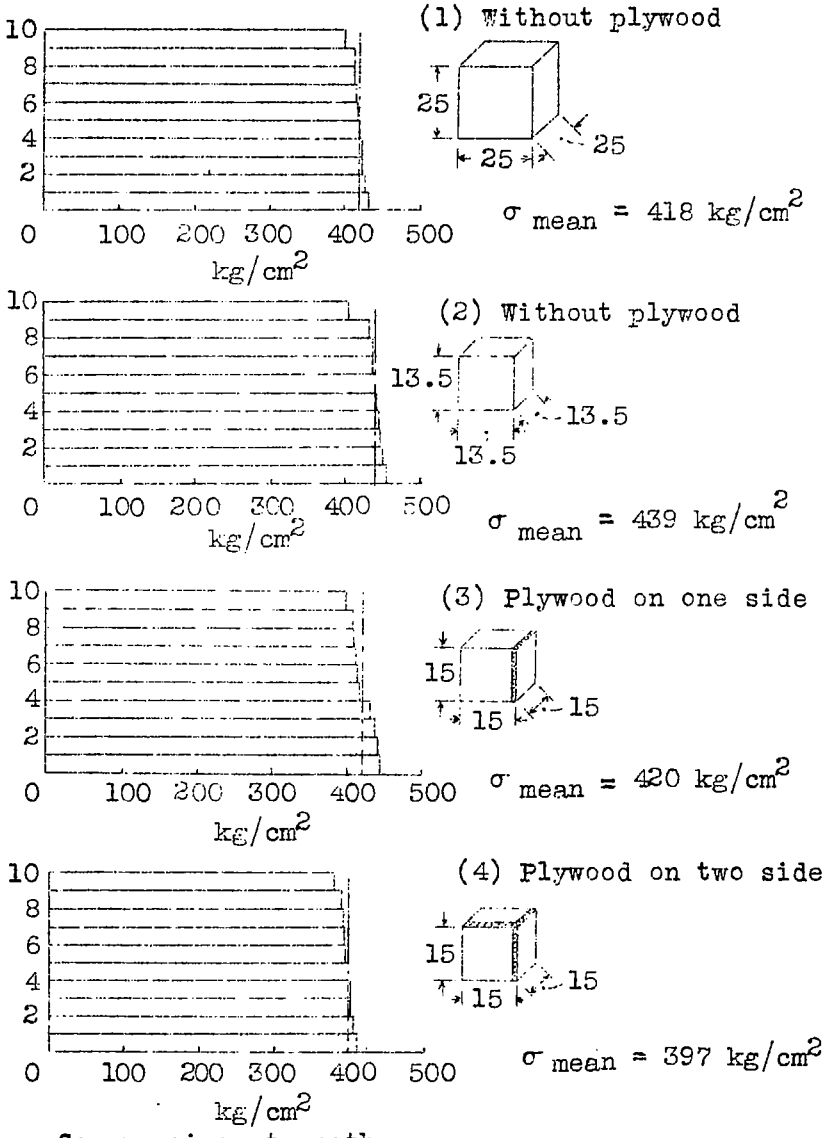

Fig. 44 Wood spar I. Compressive strength of flange material (from compression cubes). The numbers at the left show how many of the ten samples attained the correspnnding compressive strength.